Hindawi
Shock and Vibration
Volume 2022, Article ID 7372167, 21 pages
https://doi.org/10.1155/2022/7372167

*Research Article*

# Free Vibration Analysis of Bulkhead-Stiffened Functionally Graded Open Shell Using a Meshless Method

**Songhun Kwak**,[1] **Kwanghun Kim**,[2] **Kyongjin Pang**,[3] **Sok Kim**,[4] **and Pyol Kim**[5]

[1]*Department of Mechanical Science and Technology, Kim Chaek University of Technology, Pyongyang 950003, Democratic People's Republic of Korea*
[2]*Department of Mechanical Engineering, Pyongyang University of Mechanical Engineering, Pyongyang 999093, Democratic People's Republic of Korea*
[3]*Department of Organic Chemistry, Hamhung University of Chemical Engineering, Hamhung, Democratic People's Republic of Korea*
[4]*Department of Information Engineering, Chongjin Mine and Metal University, Chongjin 999091, Democratic People's Republic of Korea*
[5]*Faculty of Geology, Kim Il Sung University, Pyongyang 999093, Democratic People's Republic of Korea*

Correspondence should be addressed to Kwanghun Kim; kimkwanghun@163.com

Received 26 May 2022; Revised 11 July 2022; Accepted 4 August 2022; Published 1 September 2022

Academic Editor: Vasudevan Rajamohan



This paper focuses on the free vibration analysis of bulkhead-stiffened functionally graded open shell (FGOS) by means of the first-order shear deformation theory (FSDT) and the meshless strong form method. The bulkhead-stiffened FGOS is decomposed into several segments without bulkhead, and the equations of motion and boundary conditions for each segment are discretized by meshless strong form method, and the displacement components are approximated using meshfree Legendre–RIPM shape function using the combined basis of multi-quadrics (MQ) radial function and Legendre polynomials. The continuous conditions of displacement are applied at the interfaces between segments. The boundary and continuous conditions are enforced by using the artificial spring technique. The accuracy and reliability of the current method are validated by comparing the present results with those of the kinds of literature and the finite element program ABAQUS. The effects of some geometrical parameters and boundary conditions on the natural frequencies of bulkhead-stiffened FGOS are investigated through numerical examples, which may serve as benchmark data.

## 1. Introduction

Functional grade materials (FGMs) are special composites whose material properties change smoothly and continuously from one surface to another, usually created by mixing two or more phases of materials for specific design requirements. In particular, a mixture of ceramic and metal can take advantage of desirable properties such as the heat and corrosion resistance of ceramic and high tensile strength, toughness, and bonding ability of metal. Developing an effective method to more accurately calculate the natural frequency, which is the basic dynamic parameter of the functionally graded shell and plate, has always been the focus of scholars' research. In the past, many studies were conducted to determine the natural frequencies and mode shapes of various functionally graded shells and plates. Su et al. [1] presented the free vibration analysis of functionally graded open cylindrical, conical and spherical shells with arbitrary circumferential included angle and general boundary conditions. It was assumed that the material properties of the open shells varied continuously and smoothly in the thickness direction based on general four-parameter power-law distributions. An exact analytical solution for free vibration analysis of a moderately thick functionally graded annular sector plate was presented by Saidi et al. [2]. Rouzegar and Abad [3] presented an

analytical solution for free vibration analysis of a functionally graded plate integrated with piezoelectric layers using a four-variable refined plate theory. Chakraverty and Pradhan [4] investigated free vibration characteristics of functionally graded rectangular plates subject to different boundary conditions within the framework of classical or Kirchhoff's plate theory. Natarajan et al. [5] studied the linear free flexural vibrations of FGM plates with a through center crack using an 8-noded shear flexible element. In their study, the Mori–Tanaka homogenization scheme was used to estimate the effective material properties. Many studies have been conducted on the dynamic analysis of coupled shells and plates with various geometries, which are widely used in practical applications [6–8]. Bagheri et al. [9] presented the free vibration analysis for a FGM conical-spherical shell by using the semi analytical generalized differential quadrature method. In their study, governing equations of the shell system were established using the continuity conditions of displacement components at the intersection between the conical and spherical shells. Wang et al. [10] investigated the free vibration characteristics of irregular elastic coupled plate systems by means of Chebyshev–Ritz method, in which the coupling conditions between each plate were simulated by artificial virtual springs. The theories on which studies for the analysis of static and dynamic characteristics of composite plates and shells are based can be classified into two types: two-dimensional theory and three-dimensional theory [11–14]. Two-dimensional theories include classical plate theory (CPT) [15–17], FSDT [18, 19], and high order shear deformation theory (HSDT) [20–23]. Two-dimensional theories are based on the Kirchhoff hypothesis that normal to the middle surface remains normal to it during deformations and such assumptions are characterized by the middle surface displacements [24]. The advantage of two-dimensional theory over three-dimensional theory is that it reduces the dimension of governing equations, which greatly decreases the computational cost. In particular, FSDT is widely used in formulations for static and dynamic analysis of different plates and shells because of its high accuracy and low computational cost. Qu et al. [25] derived a general formulation for free, steady-state, and transient vibration analyses of functionally graded shells of revolution by means of a modified variational principle in conjunction with a multi-segment partitioning procedure on the basis of the FSDT. Xie et al. [26] presented a Haar wavelet discretization (HWD) method-based solution approach for the free vibration analysis of functionally graded spherical and parabolic shells of revolution with arbitrary boundary conditions on the basis of FSDT. Natarajan et al. [19] used the FSDT in order to study the flutter behavior of functionally graded material plates immersed in a supersonic flow. For static and dynamic analysis of various plates and shells, several effective methods including semi analytical method [27], spectral-Tchebychev solution technique [28], Chebyshev–Ritz method [29], Fourier series solution method [30], and finite element method [31–34] have been applied. Ye et al. [35] developed a general classical shell theory in conjunction with Chebyshev polynomials and Rayleigh–Ritz procedure for the free vibration analysis of open shells subjected to arbitrary boundary conditions. Xue et al. [36] conducted the free vibration analysis of porous square plate, circular plate, and rectangle plate with a central circular hole in the framework of isogeometric analysis (IGA). The dynamic stiffness method (DSM) is applied for free vibration analysis of thin functionally graded rectangular plates by Kumar et al. [37]. Talebitooti and Anbardan [38] investigated the free vibrational characteristics of the generally doubly curved shells of revolution by means of an explicit method based on the HWD approach. Studies were also conducted to apply the meshless method to the dynamic analysis of plates and shells. The meshless methods use a set of nodes scattered within the problem domain and on the boundaries to represent the problem domain and its boundaries [39]. In meshless method, the nodes do not form a mesh, meaning it does not require any a priori information on the relationship between the nodes for the approximation of the unknown functions. Zarei and Khosravifard [40] investigated the vibrational behavior of prestressed laminated plates by means of meshless radial point interpolation method (RPIM). Fallah and Delzendeh [41] proposed a meshless finite volume (MFV) method for free vibration analysis of laminated composite plates. In their study, moving least square (MLS) shape function was used to approximate field variables. Vu et al. [42] presented a numerical method based on the moving Kriging (MK) interpolation meshless method for analysis of static bending, free vibration, and buckling of functionally graded (FG) plates. Zhang et al. [43] investigated the free vibration characteristics of functionally graded nanocomposite triangular plates reinforced by single-walled carbon nanotubes using the element-free IMLS-Ritz method. The bulkhead-stiffened shells, which achieve high stiffness and low weight properties by connecting thin plates to various shell structures, are widely used in various industries including ship and aerospace. When the plate is attached to the conical shell, the dynamic properties of the coupled system change significantly, and the frequency response also changes [44]. Therefore, it is an important issue to develop a calculation method for the dynamic characteristics analysis of the bulkhead-stiffened shells. Qu et al. [45] developed a semi analytical method to predict the vibration and acoustic responses of submerged coupled spherical-cylindrical-spherical shells stiffened by circumferential rings and longitudinal stringers. Chen et al. [46] presented a wave-based method that can be recognized as a semi analytical and semi numerical method to analyze the free vibration characteristics of ring stiffened cylindrical shells with intermediate large frame ribs. Through literature review, it can be seen that there are very few studies on the free vibration analysis of FGOS stiffened with wide bulkheads. Moreover, the stiffeners were not considered as individual structures, and the bulkhead-stiffened shells were treated as a structure with reinforced stiffness. However, if the geometric dimensions of the stiffeners are relatively large, the stiffness conversion method cannot be applied.

The purpose of this paper is to analyze the free vibration characteristics of the FGOS with axial or circumferential bulkheads using meshless strong form method. A bulkhead-

stiffened FGOS is decomposed into several shells and bulkheads, and each segment are transformed into square plates through the coordinate mapping technique. The governing equations and boundary conditions of each segment derived by FSDT and Hamilton's principle are discretized using meshless strong form method. In this paper, a Legendre-RIPM shape function is employed to approximate the displacement components of equations. The Legendre-RIPM shape function uses the combined basis of the Legendre polynomial and the MQ radial basis function [47]. Radial basis functions are powerful tools for multivariate scattered data interpolation and have enjoyed considerable research in recent decades [48]. Legendre polynomials are chosen because they have exponential convergence behavior and superior numerical stability and accuracy. The convergence of the proposed method is investigated, and the reliability and accuracy are verified through comparison with the results of kinds of literature and finite element software ABAQUS. The effects of the geometry of bulkhead and boundary conditions on the frequency parameters of FGOS are investigated through numerical examples.

## 2. Theoretical Formulations

In this section, the bulkhead-stiffened FGOS is decomposed into several open shells and bulkheads, and the governing equations and boundary conditions of each segment are derived by the FSDT and Hamilton's principle. The governing equations of the entire system are obtained using the continuous conditions of displacement components at the interfaces between the segments, and the displacement components in the equations are approximated by the meshless Legendre-RPIM shape function.

*2.1. Description of the Model.* Figure 1 shows the geometry and coordinate system of bulkhead-stiffened FGOS. In Figure 1(a), $L_1$, $\theta_1$, and $\theta_2$ are the axial and circumferential sizes of FGOS. The symbols $\alpha$, $R$ and $h$ denote the semi vertex angle, small edge radius, and thickness of the shell, respectively. The FGOS is stiffened with a rectangular plate of length $L_1$ and height $d$. In Figure 1(b), the FGOS is stiffened using two annular or conical open shells. In this study, the bulkhead-stiffened FGOS is decomposed into several segments, and orthogonal coordinate systems ($x$, $\beta$, and $z$) are introduced into the middle surfaces of the segments.

From the assumption that each segment of FGOS is made of a mixture of ceramic and metal, the effective material properties are proportional to the volume fraction $V_c$ [1].

$$E = (E_c - E_m)V_c + E_m, \mu = (\mu_c - \mu_m)V_c + \mu_m, \rho = (\rho_c - \rho_m)V_c + \rho_m, \tag{1}$$

where $E$, $\mu$, and $\rho$ are Young's modulus, Poisson's ratios, and mass density of the functionally graded material, respectively. The indices $c$ and $m$ describe the ceramic and metallic constituents.

In this study, the volume fraction is expressed as follows:

$$V_c = \begin{cases} \left[1 - a\left(0.5 + \dfrac{z}{h}\right) + b\left(0.5 + \dfrac{z}{h}\right)^c\right]^p : \mathrm{FGM_I}, \\ \left[1 - a\left(0.5 - \dfrac{z}{h}\right) + b\left(0.5 - \dfrac{z}{h}\right)^c\right]^p : \mathrm{FGM_{II}}, \end{cases} \tag{2}$$

where $p$ is the power law index. The symbols $a$, $b$, and $c$ denote the parameters of the material composition in the thickness direction.

*2.2. Governing Equations and Boundary Conditions for Each Segment.* Based on the assumption of FSDT, the displacement components of moderately thick FGOS are expressed as follows [25]:

$$\begin{cases} \overline{u}(x, \beta, z, t) = u(x, \beta, t) + z\psi_x(x, \beta, t), \\ \overline{v}(x, \beta, z, t) = v(x, \beta, t) + z\psi_\beta(x, \beta, t), \\ \overline{w}(x, \beta, z, t) = w(x, \beta, t), \end{cases} \tag{3}$$

where $t$ is time variable, and $\overline{u}$, $\overline{v}$, and $\overline{w}$ are the generalized displacements in the $x$, $\beta$, and $z$ directions, respectively. The symbols $u$, $v$, and $w$ represent the translating displacements along $x$, $\beta$, and $z$ directions on the middle surface, respectively. Besides, $\psi_x$ and $\psi_\beta$ are the rotations of transverse normal with respect to $\beta$ and $x$-axes.

Meanwhile, the matrix form of the displacement-strain relationship of a moderately thick FGOS can be expressed as follows:

$$\boldsymbol{\varepsilon} = \mathbf{B}\mathbf{u}, \tag{4}$$

where $\varepsilon$ is a strain vector, which is composed of the middle surface strains and the curvature changes.

$$\boldsymbol{\varepsilon} = \left[\, \varepsilon_x^0 \;\; \varepsilon_\beta^0 \;\; \gamma_{x\beta}^0 \;\; \chi_x \;\; \chi_\beta \;\; \chi_{x\beta} \;\; \gamma_{\beta z}^0 \;\; \gamma_{xz}^0 \,\right]^T, \tag{5}$$

where $\varepsilon_i^0$ and $\gamma_{ij}^0$ denote the normal and shear strains; $\chi_i$ and $\chi_{ij}$ are the curvature and twist changes. In equation (4), $u$ and $B$ represent the displacement vector in the middle surface and the partial differential operator matrix, respectively.

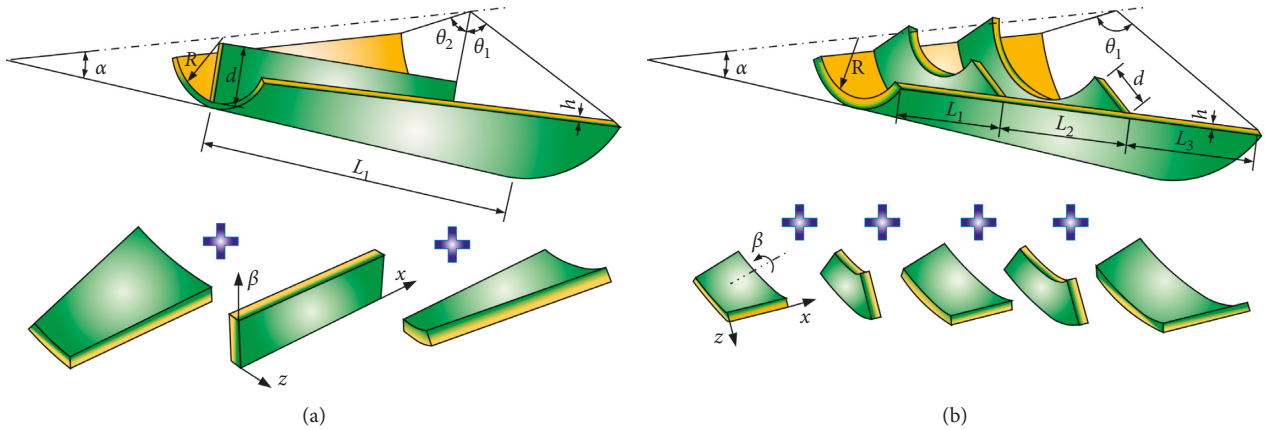


FIGURE 1: The geometry of bulkhead-stiffened functionally graded open conical shell (a) axial bulkhead (b) circumferential bulkhead.

$$\mathbf{u} = \begin{bmatrix} u & v & w & \psi_x & \psi_\beta \end{bmatrix}^T,$$

$$\mathbf{B} = \begin{bmatrix} \frac{\partial}{\partial x} & P & Q\frac{\partial}{\partial \beta} & 0 & 0 & 0 & 0 & 0 \\ 0 & Q\frac{\partial}{\partial \beta} & \frac{\partial}{\partial x} - P & 0 & 0 & 0 & -S & 0 \\ 0 & S & 0 & 0 & 0 & 0 & Q\frac{\partial}{\partial \beta} & \frac{\partial}{\partial x} \\ 0 & 0 & 0 & \frac{\partial}{\partial x} & P & Q\frac{\partial}{\partial \beta} & 0 & 1 \\ 0 & 0 & 0 & 0 & Q\frac{\partial}{\partial \beta} & \frac{\partial}{\partial x} - P & 1 & 0 \end{bmatrix}^T. \tag{6}$$

In the abovementioned equation, the symbols $P$, $Q$, and $S$ are as follows:

$$\begin{cases} P = \dfrac{\sin\alpha}{R}, Q = \dfrac{1}{R}, S = \dfrac{\cos\alpha}{R}: & \text{Conical shell,} \\ P = S = 0, Q = 1: & \text{Rectangular plate.} \end{cases} \tag{7}$$

The matrix form of the internal force-strain relationship of a moderately thick FGOS can be expressed as follows:

$$\mathbf{N} = \mathbf{D}\boldsymbol{\varepsilon}, \tag{8}$$

where the internal force vector $N$ is as follows:

$$\mathbf{N} = \begin{bmatrix} N_x & N_\beta & N_{x\beta} & M_x & M_\beta & M_{x\beta} & Q_\beta & Q_x \end{bmatrix}^T, \tag{9}$$

where $N_i$ and $N_{ij}$ indicate the normal and shear internal forces; $M_i$ and $M_{ij}$ are the bending and twisting moments, respectively. In addition, $Q_i$ is the transverse shear force. In (8), the symbol $D$ represents the material property matrix of the FGOS.

$$\mathbf{D} = \begin{bmatrix} A_{11} & A_{12} & 0 & B_{11} & B_{12} & 0 & 0 & 0 \\ A_{12} & A_{11} & 0 & B_{12} & B_{11} & 0 & 0 & 0 \\ 0 & 0 & A_{66} & 0 & 0 & B_{66} & 0 & 0 \\ B_{11} & B_{12} & 0 & D_{11} & D_{12} & 0 & 0 & 0 \\ B_{12} & B_{11} & 0 & D_{12} & D_{11} & 0 & 0 & 0 \\ 0 & 0 & B_{66} & 0 & 0 & D_{66} & 0 & 0 \\ 0 & 0 & 0 & 0 & 0 & 0 & A_{44} & 0 \\ 0 & 0 & 0 & 0 & 0 & 0 & 0 & A_{55} \end{bmatrix}, \tag{10}$$

where stiffness coefficients $A_{ij}$, $B_{ij}$, and $D_{ij}$ are as follows:

$$\begin{cases} A_{ij} = \displaystyle\int_{-h/2}^{h/2} \overline{Q}_{ij} dzi, j = 1, 2, 6, \quad B_{ij} = \int_{-h/2}^{h/2} \overline{Q}_{ij} z dzi, j = 1, 2, 6, \\ A_{ii} = k_s \displaystyle\int_{-h/2}^{h/2} \overline{Q}_{ii} dzi = 4, 5, \qquad D_{ij} = \int_{-h/2}^{h/2} \overline{Q}_{ij} z^2 dzi, j = 1, 2, 6, \end{cases} \tag{11}$$

where $k_s$ is the shear correction factor, which is selected as 5/6 in this paper. The symbol $\overline{Q}_{ij}$ is the elastic stiffness coefficients.

$$\begin{aligned} \overline{Q}_{11} &= \frac{E}{1-\mu^2}, \\ \overline{Q}_{12} &= \frac{E\mu}{1-\mu^2}, \\ \overline{Q}_{44} &= \overline{Q}_{55} \\ &= \overline{Q}_{66} \\ &= \frac{E}{2(1+\mu)}. \end{aligned} \tag{12}$$

Meanwhile, according to Hamilton's principle, the matrix form of governing equations of a moderately thick FGOS is expressed as follows:

$$\mathbf{LN} + \mathbf{m}\ddot{u} = \mathbf{0}, \tag{13}$$

where $\ddot{u}$ and $\mathbf{m}$ are acceleration vector and mass matrix, respectively.

$$\ddot{u} = \left[\ddot{u}\ \ \ddot{v}\ \ \ddot{w}\ \ \ddot{\psi}_x\ \ \ddot{\psi}_\beta\right]^T,$$
$$\mathbf{m} = \begin{bmatrix} -I_0 & 0 & 0 & -I_1 & 0 \\ 0 & -I_0 & 0 & 0 & -I_1 \\ 0 & 0 & -I_0 & 0 & 0 \\ -I_1 & 0 & 0 & -I_2 & 0 \\ 0 & -I_1 & 0 & 0 & -I_2 \end{bmatrix}, \tag{14}$$

where the inertia terms are as follows:

$$[I_0, I_1, I_2] = \int_{-h/2}^{h/2} \rho\left[1, z, z^2\right] \mathrm{d}z. \tag{15}$$

In (13), the partial differential operator matrix $L$ is as follows:

$$\mathbf{L} = \begin{bmatrix} \frac{\partial}{\partial x} + P & -P & Q\frac{\partial}{\partial \beta} & 0 & 0 & 0 & 0 & 0 \\ 0 & Q\frac{\partial}{\partial \beta} & \frac{\partial}{\partial x} + 2P & 0 & 0 & 0 & S & 0 \\ 0 & -S & 0 & 0 & 0 & 0 & Q\frac{\partial}{\partial \beta} & \frac{\partial}{\partial x} + P \\ 0 & 0 & 0 & \frac{\partial}{\partial x} + P & -P & Q\frac{\partial}{\partial \beta} & 0 & -1 \\ 0 & 0 & 0 & 0 & Q\frac{\partial}{\partial \beta} & \frac{\partial}{\partial x} + 2P & -1 & 0 \end{bmatrix}. \tag{16}$$

Substituting (4) and (8) into (13)

$$\mathbf{ku} + \mathbf{m}\ddot{u} = \mathbf{0}, \tag{17}$$

where stiffness matrix $\mathbf{k}$ is

$$\mathbf{k} = \mathbf{LDB}. \tag{18}$$

The elements $L_{ij}$ of stiffness matrix $k$ are shown in Appendix A. By assuming harmonic motion, a standard characteristic equation can be achieved from (17).

$$\left(\mathbf{k} - \boldsymbol{\omega}^2\mathbf{m}\right)\mathbf{u} = 0, \tag{19}$$

where $\omega$ is natural frequency of the system.

The matrix form of boundary conditions can be expressed as follows:

$$\begin{cases} \mathbf{c_x N} - \mathbf{k}^{\mathbf{x0}}\mathbf{u} = \mathbf{0}: & \text{Left}, \\ \mathbf{c_x N} + \mathbf{k}^{\mathbf{x1}}\mathbf{u} = \mathbf{0}: & \text{Right}, \end{cases} \quad \begin{cases} \mathbf{c_\beta N} - \mathbf{k}^{\boldsymbol{\beta 0}}\mathbf{u} = \mathbf{0}: & \text{Bottom}, \\ \mathbf{c_\beta N} + \mathbf{k}^{\boldsymbol{\beta 1}}\mathbf{u} = \mathbf{0}: & \text{Top}, \end{cases} \tag{20}$$

where the mapping matrices $c_x$ and $c_\beta$ are as follows:

$$\mathbf{c_x} = \begin{bmatrix} 1 & 0 & 0 & 0 & 0 & 0 & 0 & 0 \\ 0 & 0 & 1 & 0 & 0 & 0 & 0 & 0 \\ 0 & 0 & 0 & 0 & 0 & 0 & 0 & 1 \\ 0 & 0 & 0 & 1 & 0 & 0 & 0 & 0 \\ 0 & 0 & 0 & 0 & 0 & 1 & 0 & 0 \end{bmatrix},$$
$$\mathbf{c_\beta} = \begin{bmatrix} 0 & 0 & 1 & 0 & 0 & 0 & 0 & 0 \\ 0 & 1 & 0 & 0 & 0 & 0 & 0 & 0 \\ 0 & 0 & 0 & 0 & 0 & 0 & 1 & 0 \\ 0 & 0 & 0 & 0 & 0 & 1 & 0 & 0 \\ 0 & 0 & 0 & 0 & 1 & 0 & 0 & 0 \end{bmatrix}. \tag{21}$$

The spring stiffness matrices $k_{ij}$ ($i = x, \beta$; $j = 0, 1$) are as follows:

$$\mathbf{k^{ij}} = \begin{bmatrix} k_u^{ij} & 0 & 0 & 0 & 0 \\ 0 & k_v^{ij} & 0 & 0 & 0 \\ 0 & 0 & k_w^{ij} & 0 & 0 \\ 0 & 0 & 0 & k_x^{ij} & 0 \\ 0 & 0 & 0 & 0 & k_\beta^{ij} \end{bmatrix}, \tag{22}$$

where $k_u^{ij}$, $k_v^{ij}$, $k_w^{ij}$, $k_x^{ij}$, and $k_\beta^{ij}$ denote stiffness values of boundary spring.

Substituting (4) and (8) into (20),

$$\mathbf{C_i u} = \mathbf{0}, \tag{23}$$

where the matrix $C_i$ $(i = x, \beta)$ is as follows:

$$\mathbf{C_i} = \mathbf{c_i DB} \pm \mathbf{k^{ij}}, \tag{24}$$

where the elements of matrix $\mathbf{C_i}$ are shown in Appendix B.

### 2.3. Meshless Discretization

*2.3.1. Legendre-RPIM Shape Function.* The Legendre-RPIM shape function uses a combined basis of the MQ radial functions and the Legendre polynomials [47]. The displacement $u(x)$ of a point $x$ in problem domain is approximated by the Legendre-RPIM shape function as follows:

$$\begin{aligned} u(\mathbf{x}) &= \sum_{i=1}^{n} R_i(\mathbf{x}) a_i + \sum_{j=1}^{m} L_j(\mathbf{x}) b_j \\ &= \mathbf{R^T}(\mathbf{x})\mathbf{a} + \mathbf{L^T}(\mathbf{x})\mathbf{b}, \end{aligned} \tag{25}$$

where $R_i(x)$ and $n$ are the MQ radial basis function and its number, $L_j(x)$ and $m$ are the Legendre polynomials and its number, respectively. The unknown coefficient vectors $a$ and $b$ are as follows:

$$\begin{aligned} \mathbf{a} &= \{ a_1 \;\; a_2 \;\; \dots \;\; a_n \}^T, \\ \mathbf{b} &= \{ b_1 \;\; b_2 \;\; \dots \;\; b_m \}^T. \end{aligned} \tag{26}$$

In the two-dimensional domain, Legendre polynomial basis function is expressed as Kronecker product of one-dimensional basis functions.

$$\mathbf{L}(x, y) = \left\{ L_0(x) \;\; \cdots \;\; L_j(x) \;\; \cdots \right\}^T \otimes \left\{ L_0(y) \;\; \cdots \;\; L_j(y) \;\; \cdots \right\}^T, \tag{27}$$

where $L_j(x)$ is a one-dimensional Legendre polynomial.

$$L_j(x) = \frac{1}{2^j j!} \frac{d^j}{dx^j}\left(x^2 - 1\right)^j, \; j = 0, 1, 2 \dots. \tag{28}$$

The abovementioned equation can be applied in the interval of $x \in (-1, 1)$. Therefore, in general, in order to approximate the displacements using the Legendre polynomial, the two-dimensional domain must be transformed into a square domain through coordinate mapping technique [28].

In (25), the MQ radial function $R_i$ can be written as follows:

$$R_i(x, y) = \left(r_i^2 + \kappa^2 d_a^2\right)^\eta, \tag{29}$$

where $\kappa$ and $\eta$ are the shape parameters of MQ radial basis function. $d_a$ and $r_i$ are the average nodal spacing and the distance between the point of interest and a node, respectively.

The unknown vectors $a$ and $b$ can be determined by applying equation (27) to be satisfied at $n$ nodes included in the support domain. The matrix form of the $n$ linear equations is expressed as follows:

$$\mathbf{u}_s = \mathbf{R}_0 \mathbf{a} + \mathbf{L}_m \mathbf{b}, \tag{30}$$

where the symbol $\mathbf{u}_s$ describes a vector composed of $n$ displacement components. The moment matrix of radial basis functions $R_0$ and the polynomial moment matrix $L_m$ are as follows:

$$\begin{aligned} \mathbf{R}_0 &= \begin{bmatrix} R_1(r_1) & R_2(r_1) & \cdots & R_n(r_1) \\ R_1(r_2) & R_2(r_2) & \cdots & R_n(r_2) \\ \vdots & \vdots & \ddots & \vdots \\ R_1(r_n) & R_2(r_n) & \cdots & R_n(r_n) \end{bmatrix}, \\ \mathbf{L}_m &= \left[ \mathbf{L}(x_1, y_1) \;\; \mathbf{L}(x_2, y_2) \;\; \cdots \;\; \mathbf{L}(x_n, y_n) \right]^T. \end{aligned} \tag{31}$$

In equation (33), $r_k$ in $R_i$ $(r_k)$ is the distance between the $i$-th and $k$-th nodes.

Since there are $n + m$ variables in equation (32), $m$ equations are added using the following constraint conditions:

$$\sum_{i=1}^{n} L_j(\mathbf{x}_i) a_i = \mathbf{L}_m^T \mathbf{a} = 0, \quad j = 1, 2, \dots, m. \tag{32}$$

Combining (30) and (32) yields the following set of equations:

$$\begin{aligned} \overline{u}_\mathbf{s} &= \begin{Bmatrix} \mathbf{u_s} \\ \mathbf{0} \end{Bmatrix} \\ &= \begin{bmatrix} \mathbf{R}_0 & \mathbf{L_m} \\ \mathbf{L_m^T} & \mathbf{0} \end{bmatrix} \begin{Bmatrix} \mathbf{a} \\ \mathbf{b} \end{Bmatrix} \\ &= \mathbf{G}\mathbf{a}_0. \end{aligned} \tag{33}$$

From the abovementioned equation,

$$\mathbf{a}_0 = \{ \mathbf{a} \;\; \mathbf{b} \}^T = \mathbf{G}^{-1} \overline{u}_s. \tag{34}$$

Substituting (34) into (25),

$$u(x, y) = \left\{ \mathbf{R}^T(x, y) \;\; \mathbf{L}^T(x, y) \right\} \mathbf{G}^{-1} \overline{u}_s = \overline{\Phi}^T(\mathbf{x}) \overline{u}_s, \tag{35}$$

where the original Legendre-RPIM shape function is expressed as follows:

$$\begin{aligned} \overline{\Phi}^T(x) &= \left\{ \mathbf{\Phi}^T(x, y) \;\; \mathbf{\Phi}_m^T(x, y) \right\}^T \\ &= \{ \phi_1 \;\; \phi_2 \;\; \dots \;\; \phi_n \;\; \phi_{n+1} \;\; \dots \;\; \phi_{n+m} \}, \end{aligned} \tag{36}$$

where the Legendre-RPIM shape function for the nodal displacements $\Phi(x, y)$ can be written as follows:

$$\mathbf{\Phi}^T(x, y) = \{\phi_1 \ \ \phi_2 \ \ \dots \ \ \phi_n\}. \tag{37}$$

By the Legendre-RPIM shape function, the node displacements are approximated as follows:

$$\begin{aligned} u(\mathbf{x}) &= \mathbf{\Phi}^T(\mathbf{x})\mathbf{u_s} \\ &= \sum_{i=1}^{n} \phi_i u_i. \end{aligned} \tag{38}$$

*2.3.2. Discretization of Governing Equation and Boundary Condition.* Assuming that the two-dimensional domain is discretized by $N$ nodes, the displacements at node $I$ are approximated by the proposed Legendre-RPIM shape function as follows:

$$\begin{aligned} \mathbf{u}(x_I, \beta_I) &= \left\{ u^I \ \ v^I \ \ w^I \ \ \psi_x^I \ \ \psi_\beta^I \right\}^T \\ &= \mathbf{\Phi}^T(x_I, \beta_I)\mathbf{u}_s. \end{aligned} \tag{39}$$

Considering (38), the Legendre-RPIM shape function matrix $\Phi(x_I, \beta_I)$ for five displacement components at node $I$ can be written as follows:

$$\mathbf{\Phi}^T(x_I, \beta_I) = \begin{bmatrix} \phi_1 & 0 & 0 & 0 & 0 & \cdots & \phi_N & 0 & 0 & 0 & 0 \\ 0 & \phi_1 & 0 & 0 & 0 & \cdots & 0 & \phi_N & 0 & 0 & 0 \\ 0 & 0 & \phi_1 & 0 & 0 & \cdots & 0 & 0 & \phi_N & 0 & 0 \\ 0 & 0 & 0 & \phi_1 & 0 & \cdots & 0 & 0 & 0 & \phi_N & 0 \\ 0 & 0 & 0 & 0 & \phi_1 & \cdots & 0 & 0 & 0 & 0 & \phi_N \end{bmatrix}. \tag{40}$$

Similarly, displacement vector $u_s$ is as

$$\mathbf{u}_s = \left[ u_1 \ \ v_1 \ \ w_1 \ \ \psi_{x1} \ \ \psi_{\beta 1} \ \ \dots \ \ u_n \ \ v_n \ \ w_n \ \ \psi_{xN} \ \ \psi_{\beta N} \right]^T. \tag{41}$$

Substituting (39) into (19), the nodal discrete equation corresponding to node $I$ is obtained.

$$\left(\mathbf{k}_I - \omega^2 \mathbf{m}_I\right)\mathbf{u}_s = \mathbf{0}, \tag{42}$$

where the nodal stiffness matrix $k_I$ and the nodal mass matrix $m_I$ are as follows:

$$\begin{aligned} \mathbf{k_I} &= \mathbf{k}\mathbf{\Phi_I^T}, \\ \mathbf{m_I} &= \mathbf{m}\mathbf{\Phi_I^T}. \end{aligned} \tag{43}$$

Similarly, the nodal discrete equations established for all nodes in the problem domain are grouped according to the node number to obtain the stiffness matrix and mass matrix of a segment.

$$\begin{aligned} \mathbf{K_j} &= \left[ \mathbf{k}_1 \ \ \mathbf{k}_2 \ \ \dots \ \ \mathbf{k_N} \right]^T, \\ \mathbf{M_j} &= \left[ \mathbf{m}_1 \ \ \mathbf{m}_2 \ \ \dots \ \ \mathbf{m_N} \right]^T, \end{aligned} \tag{44}$$

where index $j$ denotes the number of segment.

Similarly, substituting equations (42) into (25),

$$\mathbf{C}_i \mathbf{\Phi}_k^T \mathbf{u}_s = \mathbf{0}. \tag{45}$$

The above equation means the discretized boundary condition for a node $k$ on the boundary of the $j$-th segment.

*2.4. Continuous Conditions.* If the $j$-th segment is axially connected to the left or right side of the $i$-th segment, the continuation condition can be written as

$$\mathbf{C}_x \mathbf{D}\mathbf{B}\mathbf{u}_i \pm \mathbf{k}_c\left(\mathbf{u}_i - \mathbf{u}_j\right) = \mathbf{0}, \tag{46}$$

where $u_i$ and $u_j$ are the displacement vectors in the interface between the $i$-th and $j$-th segments, respectively. The combination stiffness matrix $k_c$ is as follows:

$$\mathbf{k}_c = \begin{bmatrix} k_c & 0 & 0 & 0 & 0 \\ 0 & k_c & 0 & 0 & 0 \\ 0 & 0 & k_c & 0 & 0 \\ 0 & 0 & 0 & k_c & 0 \\ 0 & 0 & 0 & 0 & k_c \end{bmatrix}, \tag{47}$$

where $k_c$ is the combination stiffness value between the segments, which must be large enough to represent the rigid connection of the shells.

Similarly, when the $i$-th segment and the $j$-th segment are connected in the circumferential direction, the continuity condition is as follows:

$$\mathbf{C}_\beta \mathbf{D}\mathbf{B}\mathbf{u}_i \pm \mathbf{k}_c\left(\mathbf{u}_i - \mathbf{u}_j\right) = \mathbf{0}. \tag{48}$$

## 3. Numerical Results and Discussion

Based on the abovementioned derivations, some numerical examples for the free vibration of FGOS with axial and circumferential bulkheads are presented in this section. Firstly, the convergence study of the present method is performed in order to determine proper number of nodes and spring stiffness values. Secondly, the comparisons of numerical results with those of published pieces of literature and finite element software ABAQUS are performed to validate the accuracy and reliability of the present method. Finally, several numerical examples of the free vibration analysis of FGOS with various bulkheads and boundary conditions are provided. Numerical results by the proposed method are provided through self-compiled MATLAB code.

Unless otherwise stated, the bottom boundary of the bulkhead is clamped and the material properties of the FGOS are given as: $E_m = 70$ GPa, $\mu_m = 0.3$, $\rho_m = 2707$ kg/m$^3$, $E_c = 168$ GPa, $\mu_c = 0.3$, and $\rho_c = 5700$ kg/m$^3$.

*3.1. Verification and Convergence Study.* In order to solve the free vibration problem of the FGOS with various bulkheads using the meshless strong form method, the shell is divided into several segments and each segment domain is discretized by $N{=}N_x \times N_\beta$ nodes. In this paper, the segmented domain is converted to a square shape through coordinate mapping technology, so $N_x = N_\beta$ is set. In numerical methods, the number of elements or nodes directly affects the accuracy and efficiency of the results. Figure 2 shows the change in frequency parameters $\Omega = (\omega L^2/h\sqrt{\rho_c/E_c})$ according to the number of nodes $N_x$ in FGM$_\mathrm{I}$ ($a = 1/b = 0/p = 1$) open shells with axial and circumferential bulkheads.

The geometries of the shells are as follows:

FGOS with a axial bulkhead: $R = 1$ m, $L/R = 2$, $d/R = 0.5$, $h/R = 0.1$, $\theta_1 = \theta_2 = \pi/4$, and $\alpha = 0$.

FGOS with a circumferential bulkhead: $R = 1$ m, $d/R = 0.5$, $h/R = 0.1$, $L_1 = L_2 = 1$m, $\theta_1 = \pi/2$, and $\alpha = \pi/6$.

From Figure 2, it can be seen that the variations of all numerical results after $N_x = 10$ are very small. Based on these results, $N_x = 11$ is used in all the following examples.

Next, one boundary of the shell is selected as the elastic boundary and the other boundaries are fixed to study the convergence of stiffness value of boundary spring. The geometries of FGM$_\mathrm{I}$ ($a = 1/b = 0/p = 1$) open shells considered in this study are same as those in Figure 2. Figure 3 shows the variation of frequency parameters according to the spring stiffness values of elastic boundaries in FGOS with axial and circumferential bulkheads.

As can be seen in Figure 3, the variation of the frequency parameters according to $k_w$ is relatively quick in the interval of $10^6$~$10^{11}$. Thereafter, when the spring stiffness value exceeds $10^{13}$, the frequency parameters tend to be stable, which shows that the clamped boundary can be simulated.

Based on the abovementioned study, the spring stiffness value of clamped boundary is selected as $10^{14}$ in the following numerical examples. In this paper, clamped boundary, free boundary, elastic supported boundary, and simply supported boundary are considered, and the spring stiffness values of the ground according to the type of boundary conditions are shown in Table 1.

The accuracy of the proposed method for the free vibration analysis of FGOS with axial and circumferential bulkheads is verified through the comparison with the results of pieces of literature and finite element software ABAQUS. The FGOS without bulkhead is a special case of FGOS with bulkheads. Therefore, in Table 2, the fundamental frequency parameters $\Omega$ of FGM$_\mathrm{II}$ ($a = 1/b = 0$) open cylindrical shells with various sizes of thickness and radius obtained by the proposed method are compared with the results of literatures [1, 49]. The material properties of the shell are as follows: $E_m = 70$ GPa, $\mu_m = 0.3$, $\rho_m = 2707$ kg/m$^3$, $E_c = 151$ GPa, $\mu_c = 0.3$ and $\rho_c = 3000$ kg/m$^3$. Table 3 shows the fundamental frequencies of functionally graded open conical shells with various power-law indices and semi vertex angles obtained by the proposed method compared with the results of literature [1]. From Tables 2 and 3, it can be seen that the numerical results obtained by the proposed method agree well with those of the published pieces of literature.

In order to further confirm the accuracy and reliability of proposed method, the natural frequency comparisons of the FGOS with axial and circumferential bulkheads are conducted. Due to the lack of literature on the FGOS with bulkheads, these results are compared with those of the finite element software ABAQUS. In Table 4, the natural frequencies of functionally graded open cylindrical shells with a circumferential bulkhead obtained by the proposed method are compared with the results by ABAQUS. The all boundaries of bulkhead are clamped. In addition, Table 5 shows the comparison of natural frequencies of functionally graded open conical shells with two axial bulkheads obtained by the proposed method with those of ABAQUS. In the bulkheads, the bottom boundaries are free and the other boundaries are clamped. As shown in Tables 4 and 5, the natural frequency results of FGOS with bulkheads by the proposed method agree well with those of ABAQUS. Figures 4–7 show the comparison of first four mode shapes of FGOS with bulkheads with those of ABAQUS.

*3.2. Numerical Examples.* Based on the verification of the convergence and accuracy of the proposed method, in this subsection, the vibration characteristics of bulkhead-stiffened FGOS with different geometries and boundary conditions are studied. First, the effect of the geometric size and position of the bulkhead on the frequency parameters of the FGOS is investigated. Figure 8 shows the change of frequency parameters $\Omega$ according to the circumferential position of bulkhead $\varphi_1$ in FGM$_\mathrm{I}$ ($a = 1/b = 0/p = 1$) open cylindrical shell with one axial bulkhead. As can be seen in Figure 8, under CCCC, CSCS, and CFCF boundary conditions, the frequency curves are symmetric in the line $\theta_1 = 45^\circ$, but lose symmetry under other boundary conditions. In particular, the frequency curve with CSCC (CFCC) boundary condition and the frequency curve with CCCS (CCCF) boundary condition are symmetric in the line $\theta_1 = 45^\circ$, with each other. In addition, in the curves of the CSCC and CFCC boundary conditions, the maximum frequency occurs when the axial bulkhead is deflected from the center to the $S$ or $F$ boundary.

The change of fundamental frequency parameters $\Omega$ according to axial position of bulkhead $L_1$ in FGM$_\mathrm{II}$ ($a = 1/b = 0/p = 1$) open conical shell with one circumferential bulkhead is illustrated in Figure 9. As can be seen from Figure 9, as the semi vertex angle $\alpha$ increases, the fundamental frequency parameter decreases, and the fundamental frequency parameter of the shell with $\alpha = 0$ (cylindrical) is greatest when the bulkhead is at the center. However, the fundamental frequency parameter of the conical shell with $\alpha > 0$ is greatest when the bulkhead is deflected toward a large radius side from the center of the shell.

Figure 10 shows the change of frequency parameters according to the height of bulkhead $d$ in FGM ($a = 0/$

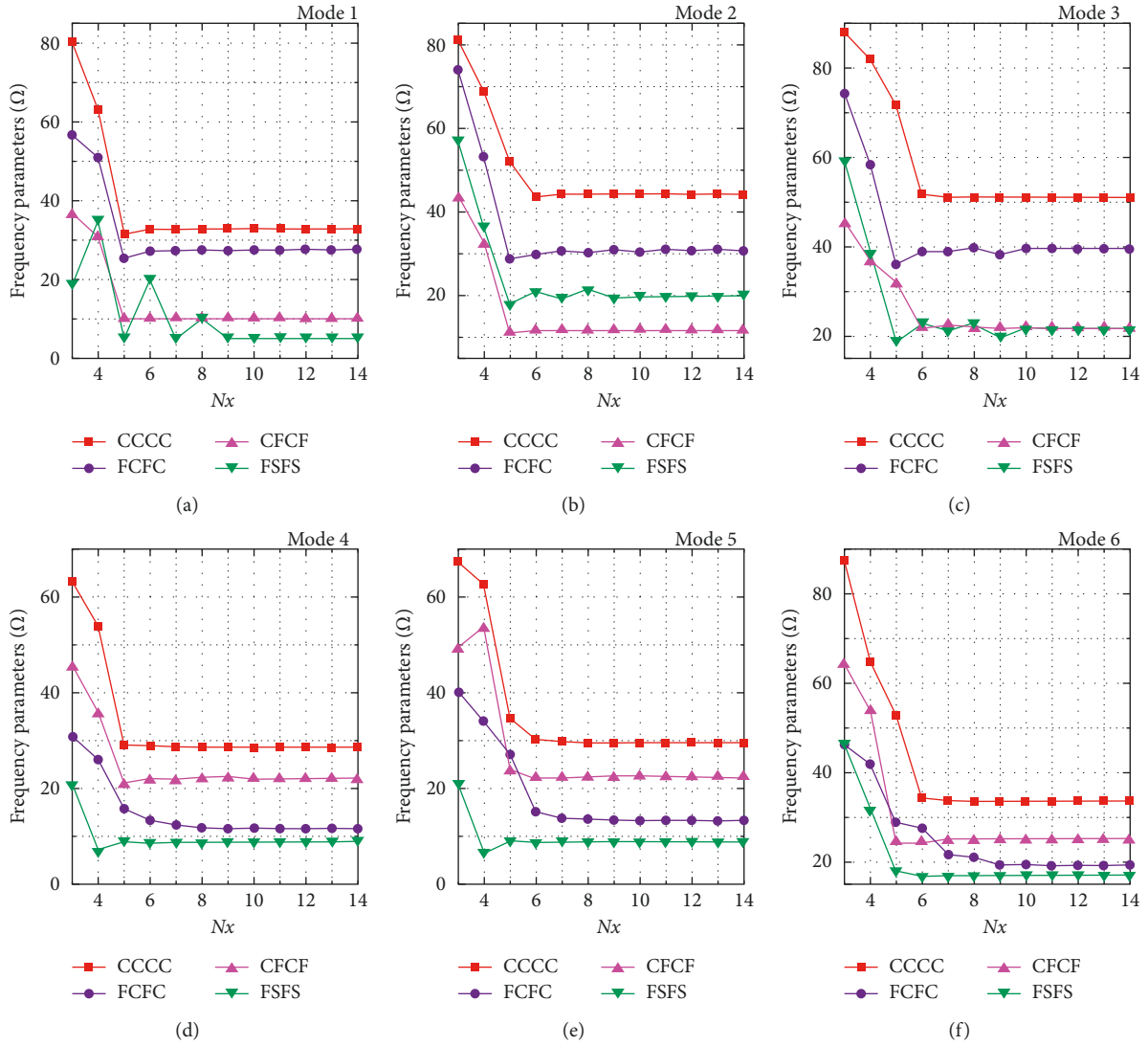


Figure 2: Variation of frequency parameters with various numbers of nodes; (a) axial bulkhead, (b) circumferential bulkhead.

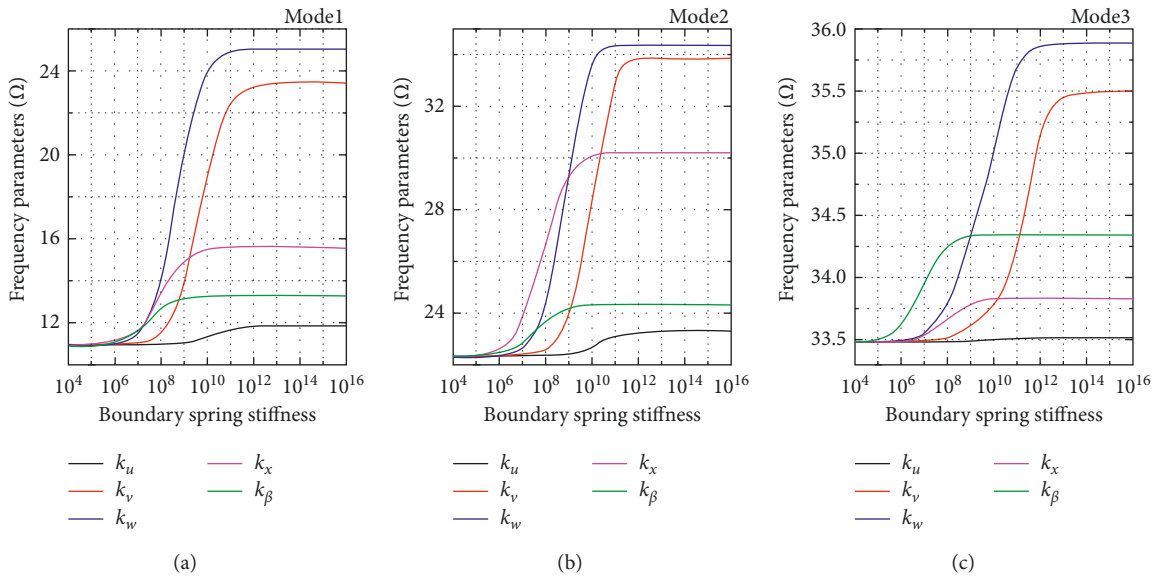


Figure 3: Continued.

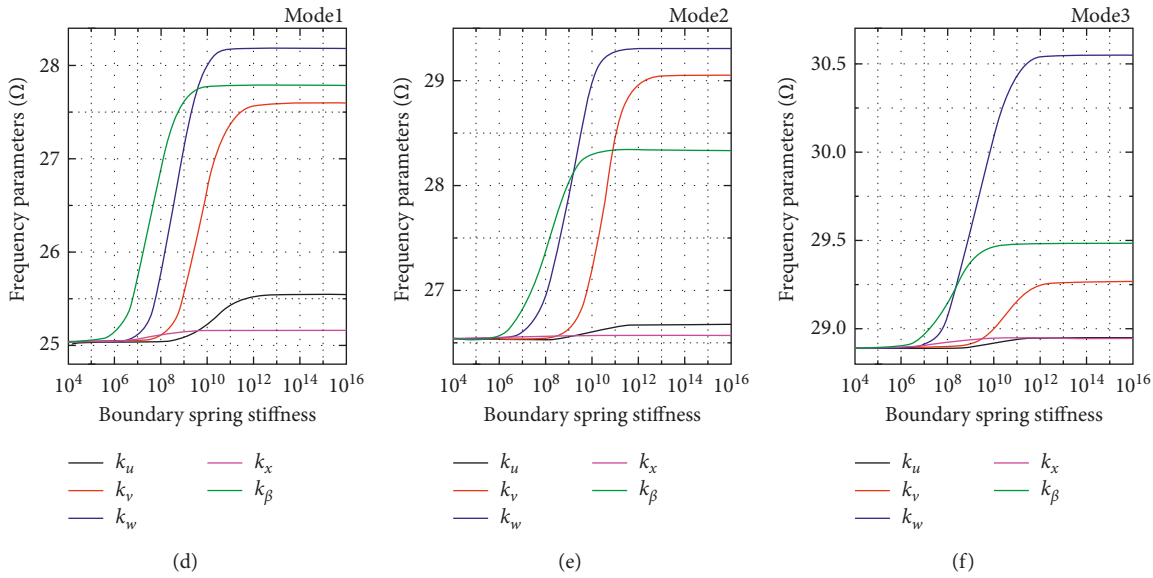


Figure 3: Variation of frequency parameters with various stiffness values of boundary springs: (a) axial bulkhead and (b) circumferential bulkhead.

Table 1: Stiffness value of boundary spring is according to the boundary condition.

| BCs | $k_u$ | $k_v$ | $k_w$ | $k_x$ | $k_\beta$ |
|---|---|---|---|---|---|
| $F$ (free) | 0 | 0 | 0 | 0 | 0 |
| $S$ (simply supported) | 0 | $10^{14}$ | $10^{14}$ | 0 | $10^{14}$ |
| $E$ (elastic supported) | $10^8$ | $10^{14}$ | $10^{14}$ | $10^{14}$ | $10^{14}$ |
| $C$ (clamped) | $10^{14}$ | $10^{14}$ | $10^{14}$ | $10^{14}$ | $10^{14}$ |

Table 2: Comparison of fundamental frequency parameters for functionally graded open cylindrical shells with SSSS boundary condition ($L = 1$m, $\theta_1 R = L$).

| $h/L$ | $R/L$ | | $p=0$ | $p=0.5$ | $p=1$ | $p=2$ | $p=5$ | $p=10$ | $p=\infty$ |
|---|---|---|---|---|---|---|---|---|---|
| 0.1 | 2 | Reference [1] | 6.1674 | 5.5622 | 5.2964 | 5.0895 | 4.9117 | 4.7787 | 4.4206 |
| | | Reference [49] | 6.1552 | 5.5522 | 5.2876 | 5.0812 | 4.9032 | 4.7700 | 4.4119 |
| | | Present | 6.1666 | 5.5615 | 5.2957 | 5.0889 | 4.9111 | 4.7781 | 4.4200 |
| | 3 | Reference [1] | 5.9517 | 5.3602 | 5.1058 | 4.9155 | 4.7568 | 4.6293 | 4.2660 |
| | | Reference [49] | 5.9456 | 5.3548 | 5.1012 | 4.9111 | 4.7524 | 4.6249 | 4.2616 |
| | | Present | 5.9509 | 5.3595 | 5.1052 | 4.9149 | 4.7562 | 4.6288 | 4.2655 |
| | 5 | Reference [1] | 5.8364 | 5.2532 | 5.0052 | 4.8241 | 4.6755 | 4.5506 | 4.1833 |
| | | Reference [49] | 5.8337 | 5.2504 | 5.0031 | 4.8220 | 4.6734 | 4.5486 | 4.1814 |
| | | Present | 5.8357 | 5.2525 | 5.0046 | 4.8235 | 4.6749 | 4.5501 | 4.1828 |
| | 10 | Reference [1] | 5.7867 | 5.2079 | 4.9632 | 4.7861 | 4.6416 | 4.5175 | 4.1477 |
| | | Reference [49] | 5.7855 | 5.2065 | 4.9622 | 4.7852 | 4.6407 | 4.5166 | 4.1469 |
| | | Present | 5.7860 | 5.2073 | 4.9625 | 4.7855 | 4.6411 | 4.5170 | 4.1472 |
| 0.02 | 2 | Reference [1] | 13.7006 | 12.5648 | 11.9635 | 11.3494 | 10.6986 | 10.3552 | 9.8201 |
| | | Reference [49] | 13.6904 | 12.5575 | 11.9578 | 11.3440 | 10.6928 | 10.3488 | 9.8128 |
| | | Present | 13.6956 | 12.5602 | 11.9592 | 11.3451 | 10.6947 | 10.3515 | 9.8167 |
| | 3 | Reference [1] | 10.1949 | 9.3158 | 8.8722 | 8.4446 | 8.0073 | 7.7589 | 7.3076 |
| | | Reference [49] | 10.1854 | 9.3077 | 8.8651 | 8.4379 | 8.0006 | 7.7522 | 7.3006 |
| | | Present | 10.1886 | 9.3100 | 8.8666 | 8.4393 | 8.0023 | 7.7542 | 7.3029 |
| | 5 | Reference [1] | 7.7722 | 7.0583 | 6.7257 | 6.4355 | 6.1600 | 5.9794 | 5.5694 |
| | | Reference [49] | 7.7616 | 7.0497 | 6.7171 | 6.4280 | 6.1525 | 5.9721 | 5.5633 |
| | | Present | 7.7631 | 7.0512 | 6.7180 | 6.4289 | 6.1535 | 5.9732 | 5.5644 |
| | 10 | Reference [1] | 6.4720 | 5.8413 | 5.5673 | 5.3596 | 5.1790 | 5.0357 | 4.6388 |
| | | Reference [49] | 6.4620 | 5.8314 | 5.5586 | 5.3502 | 5.1711 | 5.0285 | 4.6317 |
| | | Present | 6.4624 | 5.8322 | 5.5589 | 5.3505 | 5.1714 | 5.0289 | 4.6321 |

Table 3: Comparison of fundamental frequencies (Hz) for functionally graded open conical shells with various boundary conditions ($R = 1$ m, $L/R = 2$, $h/R = 0.1$, $\theta_1 = 60^\circ$).

| $\alpha$ | $p$ | CCCC | | | SCSC | | | EEEE | | |
|---|---|---|---|---|---|---|---|---|---|---|
| | | Reference [1] | Present | Diff, % | Reference [1] | Present | Diff, % | Reference [1] | Present | Diff, % |
| $FGM_I$ ($a = 1/b = 0.5/c = 2$) | | | | | | | | | | |
| | 0.5 | 509.46 | 510.54 | −0.212 | 464.13 | 466.39 | −0.487 | 337.57 | 336.80 | 0.228 |
| 30° | 1 | 507.09 | 508.18 | −0.215 | 461.94 | 464.18 | −0.485 | 336.52 | 335.69 | 0.247 |
| | 20 | 489.95 | 491.00 | −0.214 | 445.93 | 448.04 | −0.473 | 329.72 | 328.46 | 0.382 |
| | 0.5 | 307.55 | 308.61 | −0.345 | 259.31 | 261.28 | −0.760 | 260.82 | 261.05 | −0.088 |
| 60° | 1 | 306.28 | 307.34 | −0.346 | 258.22 | 260.16 | −0.751 | 259.96 | 260.16 | −0.077 |
| | 20 | 298.16 | 299.16 | −0.335 | 251.01 | 252.80 | −0.713 | 255.12 | 255.09 | 0.012 |
| $FGM_{II}$ ($a = 1/b = 0.5/c = 2$) | | | | | | | | | | |
| | 0.5 | 509.23 | 510.32 | −0.214 | 463.91 | 466.17 | −0.487 | 337.27 | 336.50 | 0.228 |
| 30° | 1 | 506.68 | 507.76 | −0.213 | 461.55 | 463.79 | −0.485 | 335.96 | 335.14 | 0.244 |
| | 20 | 489.51 | 490.55 | −0.212 | 445.50 | 447.61 | −0.474 | 329.14 | 327.88 | 0.383 |
| | 0.5 | 307.46 | 308.53 | −0.348 | 259.23 | 261.20 | −0.760 | 260.72 | 260.95 | −0.088 |
| 60° | 1 | 306.12 | 307.18 | −0.346 | 258.06 | 260.01 | −0.756 | 259.76 | 259.96 | −0.077 |
| | 20 | 297.99 | 298.99 | −0.336 | 250.85 | 252.64 | −0.714 | 254.91 | 254.88 | 0.012 |

Table 4: Comparison of first five natural frequencies (Hz) for $FGM_I$ ($a = 0/b = -0.5/c = 2/p = 2$) open cylindrical shell with a circumferential bulkhead ($R = 1$ m, $L_1 = L_2 = 1$m, $d/R = 0.5$, $\theta_1 = 90^\circ$).

| BCs | $\Omega$ | $h = 0.02$ m | | | $h = 0.05$ m | | | $h = 0.1$ m | | |
|---|---|---|---|---|---|---|---|---|---|---|
| | | FEM | Present | Diff, % | FEM | Present | Diff, % | FEM | Present | Diff, % |
| CCCC | 1 | 388.63 | 387.97 | 0.170 | 615.17 | 616.90 | −0.281 | 898.85 | 899.58 | −0.081 |
| | 2 | 400.69 | 399.89 | 0.200 | 632.40 | 631.86 | 0.085 | 915.18 | 922.85 | −0.838 |
| | 3 | 418.07 | 417.82 | 0.060 | 680.83 | 680.60 | 0.034 | 936.60 | 936.52 | 0.009 |
| | 4 | 420.33 | 419.34 | 0.236 | 700.73 | 700.56 | 0.024 | 938.06 | 940.16 | −0.224 |
| | 5 | 436.19 | 433.42 | 0.635 | 885.98 | 885.89 | 0.010 | 1347.3 | 1351.2 | −0.289 |
| CSCS | 1 | 323.30 | 321.83 | 0.455 | 497.17 | 497.13 | 0.008 | 743.80 | 743.92 | −0.016 |
| | 2 | 348.93 | 347.50 | 0.410 | 524.98 | 525.31 | −0.063 | 757.10 | 754.30 | 0.370 |
| | 3 | 371.81 | 370.94 | 0.234 | 621.40 | 618.22 | 0.512 | 760.62 | 763.44 | −0.371 |
| | 4 | 382.05 | 381.12 | 0.243 | 625.40 | 624.95 | 0.072 | 792.11 | 798.75 | −0.838 |
| | 5 | 404.78 | 405.96 | −0.292 | 635.43 | 634.71 | 0.113 | 1113.9 | 1119.6 | −0.512 |
| FCFC | 1 | 221.59 | 221.41 | 0.081 | 370.53 | 372.07 | −0.416 | 606.35 | 611.27 | −0.811 |
| | 2 | 235.37 | 236.25 | −0.374 | 375.53 | 375.67 | −0.037 | 617.56 | 618.18 | −0.100 |
| | 3 | 236.81 | 236.41 | 0.169 | 502.02 | 502.28 | −0.052 | 686.63 | 688.25 | −0.236 |
| | 4 | 252.59 | 252.26 | 0.131 | 524.64 | 524.26 | 0.072 | 709.12 | 710.18 | −0.149 |
| | 5 | 418.62 | 421.16 | −0.607 | 723.07 | 726.56 | −0.483 | 926.62 | 931.06 | −0.479 |

Table 5: Comparison of first five natural frequencies (Hz) for $FGM_I$ ($a = 0/b = -0.5/c = 2/p = 2$) opens conical shell with two axial bulkheads ($R = 1$ m, $L/R = 2$, $h/R = 0.05$, $d/R = 0.5$, $\theta_1 = \theta_2 = \theta_3 = 30^\circ$).

| BCs | $\Omega$ | $\alpha = 30^\circ$ | | | $\alpha = 45^\circ$ | | | $\alpha = 60^\circ$ | | |
|---|---|---|---|---|---|---|---|---|---|---|
| | | FEM | Present | Diff, % | FEM | Present | Diff, % | FEM | Present | Diff, % |
| CCCC | 1 | 165.01 | 165.64 | −0.382 | 160.98 | 161.71 | −0.453 | 156.33 | 156.98 | −0.416 |
| | 2 | 178.36 | 178.80 | −0.247 | 175.43 | 175.94 | −0.291 | 172.62 | 173.18 | −0.324 |
| | 3 | 289.58 | 290.47 | −0.307 | 286.22 | 287.15 | −0.325 | 267.06 | 267.55 | −0.183 |
| | 4 | 296.33 | 296.89 | −0.189 | 294.59 | 295.19 | −0.204 | 289.66 | 290.28 | −0.214 |
| | 5 | 367.51 | 368.56 | −0.286 | 311.55 | 312.26 | −0.228 | 290.06 | 290.88 | −0.283 |
| FCFC | 1 | 160.34 | 160.58 | −0.150 | 152.30 | 152.22 | 0.053 | 138.64 | 138.16 | 0.346 |
| | 2 | 176.44 | 176.62 | −0.102 | 172.30 | 172.46 | −0.093 | 165.37 | 165.32 | 0.030 |
| | 3 | 273.03 | 271.00 | 0.744 | 220.83 | 218.83 | 0.906 | 182.62 | 181.62 | 0.548 |
| | 4 | 293.65 | 293.58 | 0.024 | 252.85 | 250.91 | 0.767 | 196.83 | 195.71 | 0.569 |
| | 5 | 314.04 | 311.28 | 0.879 | 292.89 | 293.32 | −0.147 | 212.52 | 213.99 | −0.692 |
| CFCF | 1 | 116.02 | 117.02 | −0.862 | 107.16 | 108.13 | −0.905 | 98.106 | 98.794 | −0.701 |
| | 2 | 122.68 | 123.68 | −0.815 | 111.33 | 112.30 | −0.871 | 100.99 | 101.69 | −0.693 |
| | 3 | 174.34 | 174.76 | −0.241 | 167.07 | 167.62 | −0.329 | 161.37 | 161.89 | −0.322 |
| | 4 | 182.04 | 182.32 | −0.154 | 177.44 | 177.82 | −0.214 | 174.56 | 174.99 | −0.246 |
| | 5 | 257.49 | 258.40 | −0.353 | 243.34 | 244.08 | −0.304 | 229.02 | 229.50 | −0.210 |

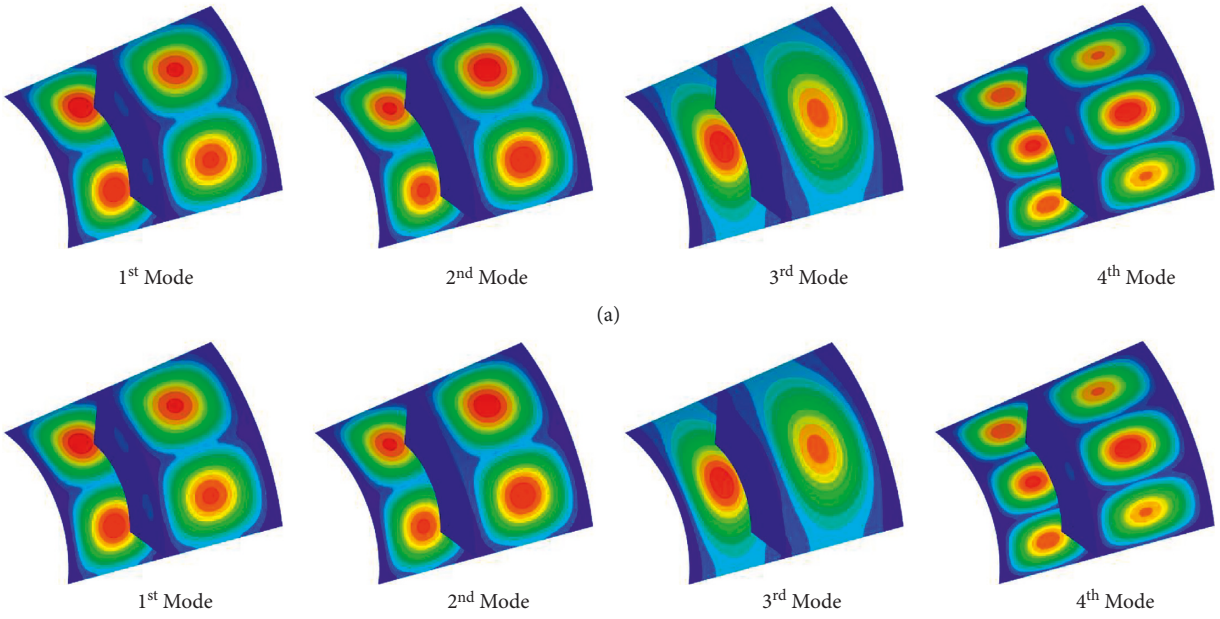


Figure 4: Mode shapes of functionally graded open cylindrical shell with a circumferential bulkhead and CSCS boundary condition ($h = 0.05$ m): (a) present and (b) ABAQUS.

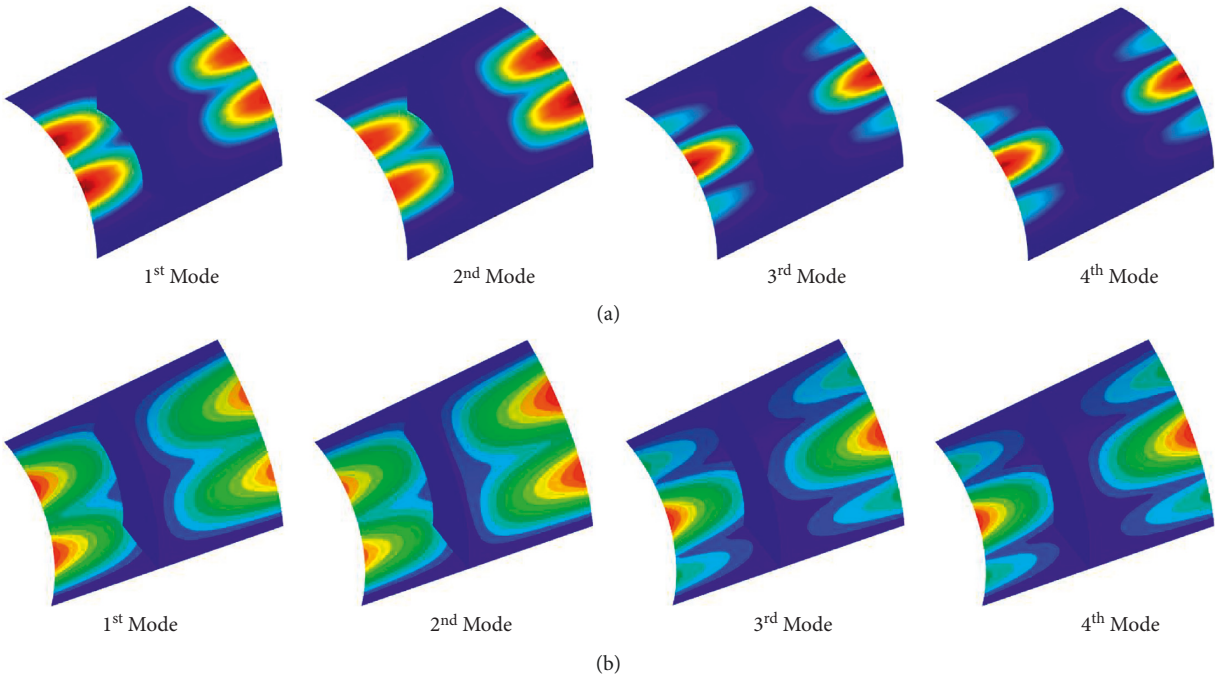


Figure 5: Mode shapes of functionally graded open cylindrical shell with a circumferential bulkhead and FCFC boundary condition ($h = 0.05$ m): (a) present and (b) ABAQUS.

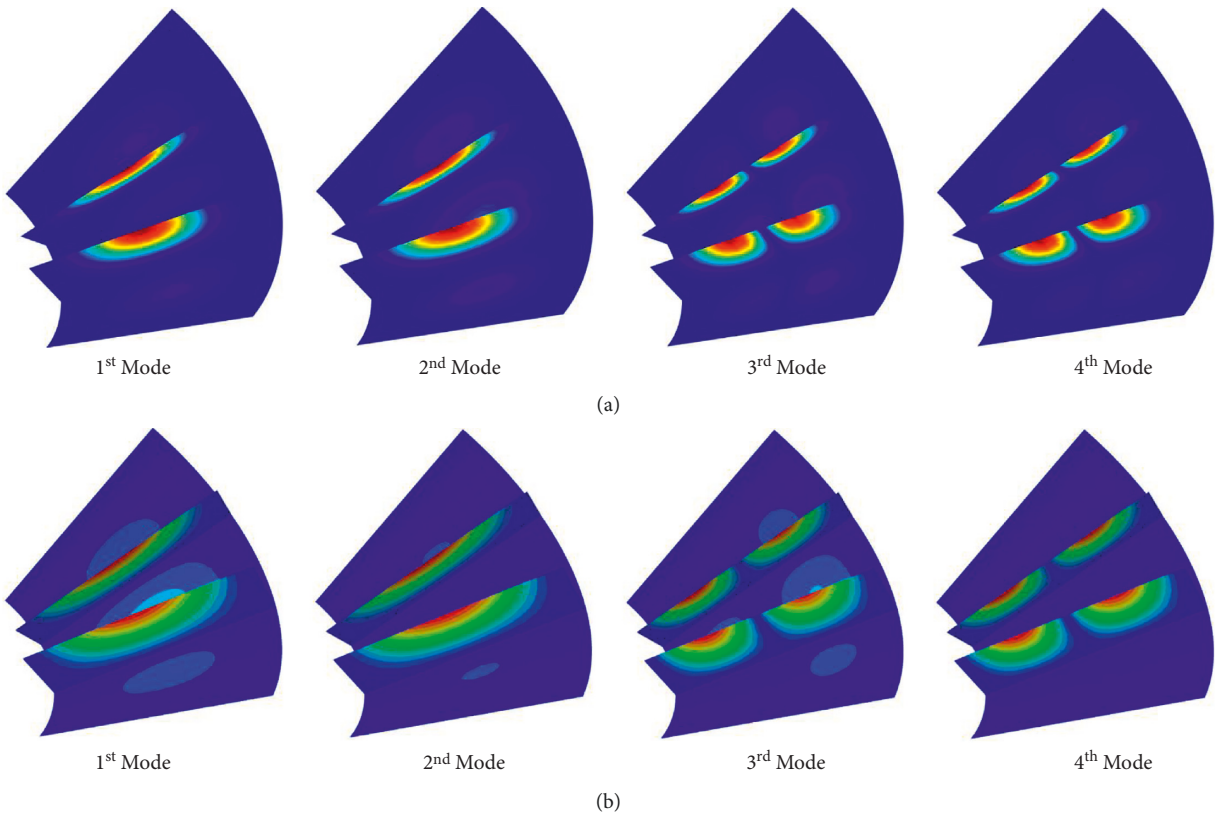


FIGURE 6: Mode shapes of functionally graded open conical shells with two axial bulkheads and CCCC boundary conditions ($\alpha = 30^{\circ}$): (a) present and (b) ABAQUS.

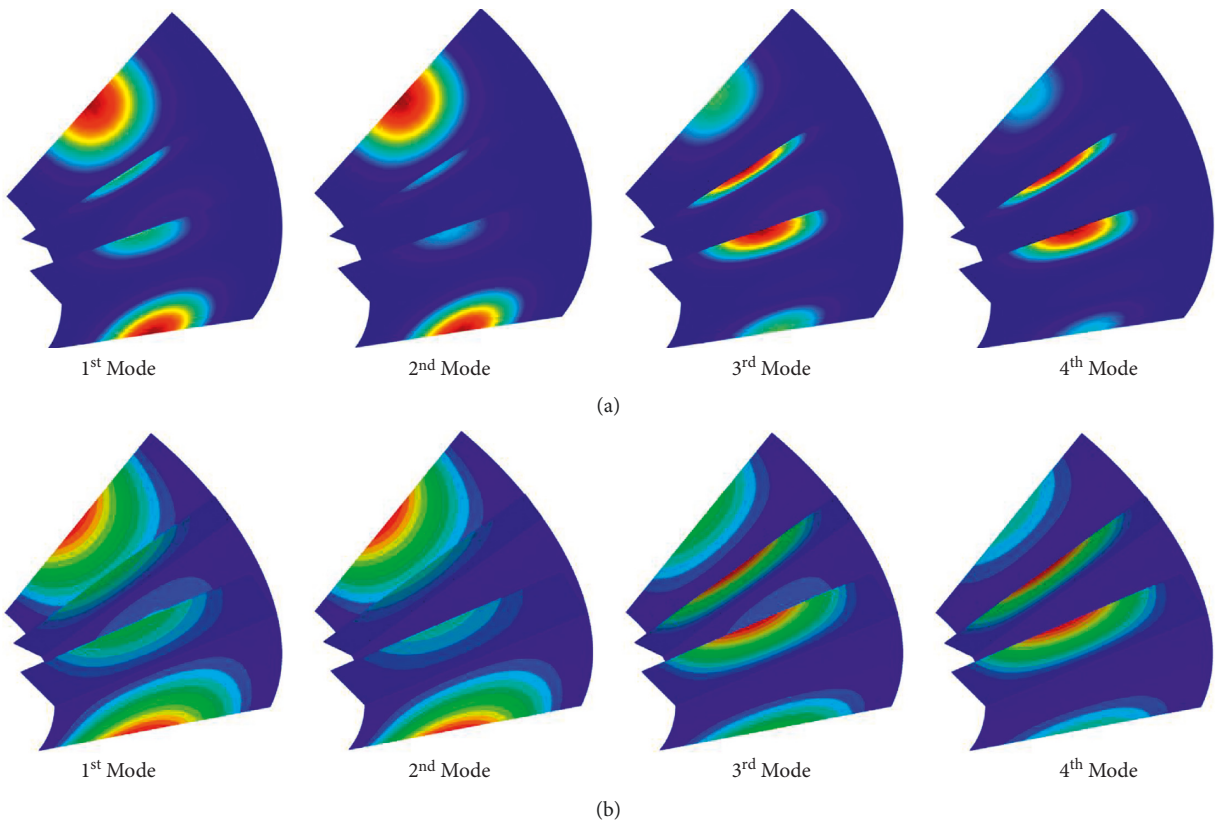


FIGURE 7: Mode shapes of functionally graded open conical shells with two axial bulkheads and CFCF boundary condition ($\alpha = 30^{\circ}$): (a) present and (b) ABAQUS.

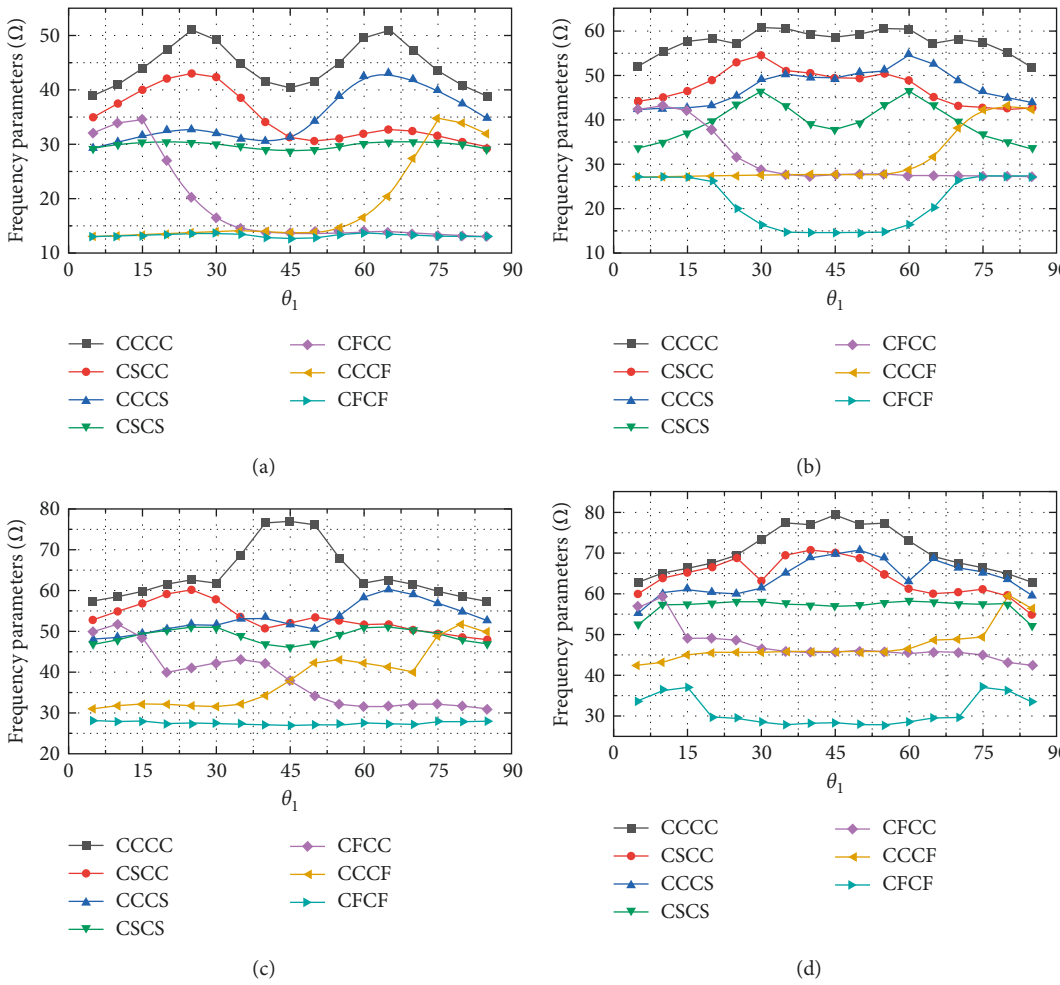


Figure 8: Variation of frequency parameters of functionally graded open cylindrical shell with an axial bulkhead according to circumferential position of bulkhead ($R = 1$ m, $L/R = 2$, $h/R = 0.05$, $d/R = 0.5$, $\theta_1 + \theta_2 = 90°$): (a) 1st mode; (b) 2nd mode; (c) 3rd mode; (d) 4th mode.

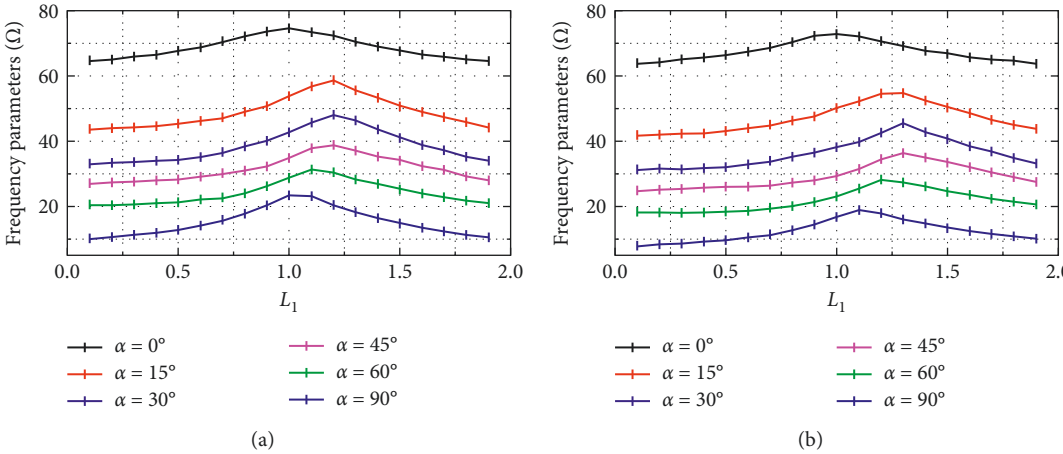


Figure 9: Continued.

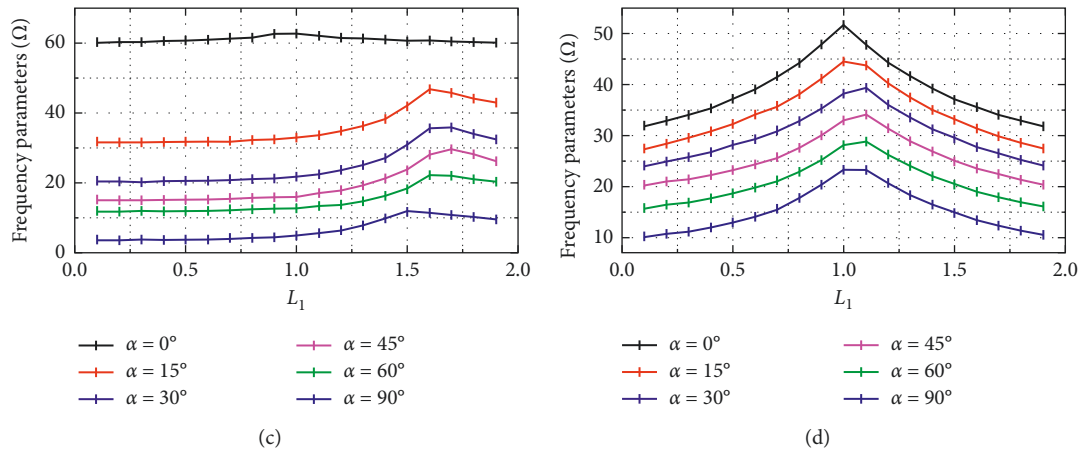


FIGURE 9: Variation of fundamental frequency parameters for functionally graded open conical shell with a circumferential bulkhead according to axial position of bulkhead ($R = 1$ m, $L_1 + L_2 = 2$ m, $h/R = 0.05$, $d/R = 0.5$, $\theta 1 = 60^{\circ}$): (a) CCCC; (b) SCSC; (c) FCFC; (d) CECE.

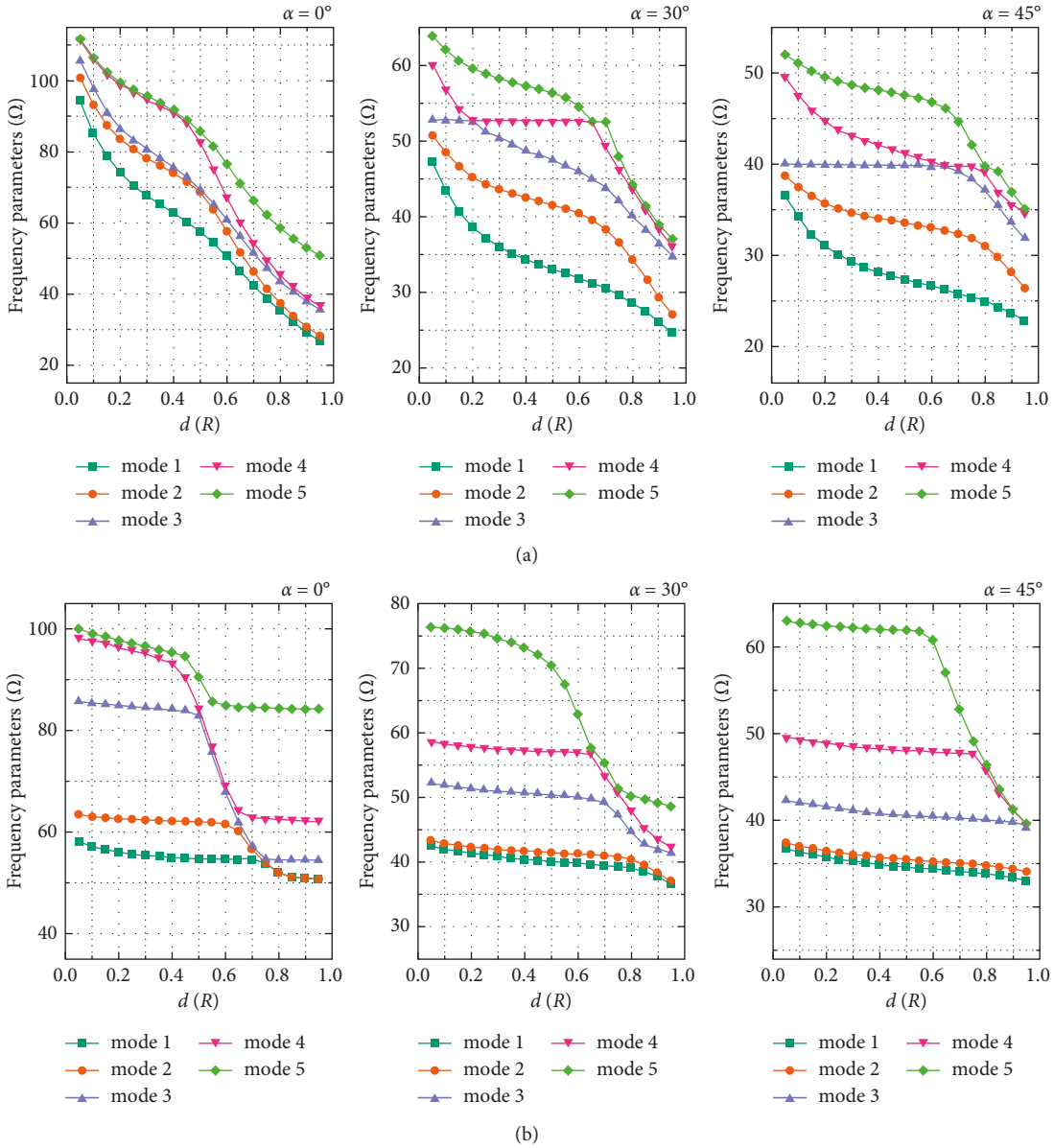


FIGURE 10: Variation of frequency parameters for FGOS with various heights of bulkheads: (a) $FGM_I$ open shell with two axial bulkheads and (b) $FGM_{II}$ open shell with two circumferential bulkheads.

Table 6: Frequency parameters for $FGM_I$ ($a = 1/b = 0$) open conical shell with one axial bulkhead and CCCC boundary condition according to power law index $p$ ($R = 1$ m, $\alpha = \pi/6$, $d/R = 0.5$, $h/R = 0.1$ m, $\theta_1 = \theta_2$).

| $L_1/R$ | $\theta_1$ | $\Omega$ | $P$ | | | | | | | |
|---|---|---|---|---|---|---|---|---|---|---|
| | | | 0 | 0.5 | 1 | 2 | 5 | 10 | 20 | $\infty$ |
| 1 | $\pi/6$ | 1 | 14.008 | 13.583 | 13.477 | 13.565 | 13.807 | 13.788 | 13.617 | 13.121 |
| | | 2 | 15.986 | 15.581 | 15.456 | 15.482 | 15.614 | 15.562 | 15.402 | 14.974 |
| | | 3 | 21.309 | 20.769 | 20.618 | 20.694 | 20.920 | 20.848 | 20.609 | 19.960 |
| | $\pi/4$ | 1 | 10.245 | 9.937 | 9.854 | 9.902 | 10.060 | 10.047 | 9.930 | 9.596 |
| | | 2 | 11.581 | 11.269 | 11.177 | 11.208 | 11.335 | 11.307 | 11.184 | 10.848 |
| | | 3 | 17.261 | 16.741 | 16.608 | 16.718 | 17.022 | 17.006 | 16.796 | 16.168 |
| | $\pi/3$ | 1 | 9.226 | 8.966 | 8.891 | 8.918 | 9.031 | 9.013 | 8.916 | 8.642 |
| | | 2 | 10.087 | 9.823 | 9.742 | 9.759 | 9.855 | 9.828 | 9.725 | 9.448 |
| | | 3 | 12.597 | 12.201 | 12.102 | 12.187 | 12.421 | 12.411 | 12.255 | 11.799 |
| | $\pi/2$ | 1 | 8.807 | 8.570 | 8.498 | 8.515 | 8.602 | 8.581 | 8.492 | 8.250 |
| | | 2 | 9.252 | 9.018 | 8.943 | 8.949 | 9.021 | 8.993 | 8.903 | 8.666 |
| | | 3 | 9.529 | 9.252 | 9.175 | 9.215 | 9.352 | 9.337 | 9.230 | 8.926 |
| 2 | $\pi/6$ | 1 | 32.965 | 31.879 | 31.615 | 31.860 | 32.531 | 32.522 | 32.109 | 30.878 |
| | | 2 | 40.475 | 39.369 | 39.052 | 39.181 | 39.652 | 39.554 | 39.118 | 37.913 |
| | | 3 | 45.224 | 43.790 | 43.432 | 43.734 | 44.579 | 44.545 | 43.991 | 42.360 |
| | $\pi/4$ | 1 | 21.352 | 20.714 | 20.539 | 20.633 | 20.953 | 20.927 | 20.687 | 20.000 |
| | | 2 | 27.848 | 27.171 | 26.951 | 26.967 | 27.166 | 27.074 | 26.799 | 26.086 |
| | | 3 | 32.790 | 31.804 | 31.536 | 31.684 | 32.184 | 32.144 | 31.775 | 30.714 |
| | $\pi/3$ | 1 | 18.372 | 17.917 | 17.766 | 17.770 | 17.897 | 17.840 | 17.666 | 17.209 |
| | | 2 | 23.681 | 23.185 | 22.997 | 22.939 | 22.972 | 22.865 | 22.662 | 22.182 |
| | | 3 | 27.672 | 26.757 | 26.538 | 26.752 | 27.332 | 27.328 | 26.974 | 25.919 |
| | $\pi/2$ | 1 | 16.739 | 16.285 | 16.150 | 16.187 | 16.355 | 16.312 | 16.143 | 15.679 |
| | | 2 | 19.188 | 18.653 | 18.505 | 18.577 | 18.744 | 18.672 | 18.493 | 17.973 |
| | | 3 | 19.268 | 18.834 | 18.682 | 18.661 | 18.834 | 18.794 | 18.576 | 18.049 |

Table 7: Frequency parameters for $FGM_{II}$ ($a = 1/b = 0$) open conical shell with one circumferential bulkhead and CCCC boundary condition according to power law index $p$ ($R = 1$ m, $\alpha = \pi/6$, $d/R = 0.5$, $h/R = 0.1$, $L_1 = L_2$).

| $\theta_1$ | $L_1/R$ | $\Omega$ | $P$ | | | | | | | |
|---|---|---|---|---|---|---|---|---|---|---|
| | | | 0 | 0.5 | 1 | 2 | 5 | 10 | 20 | $\infty$ |
| $\pi/4$ | 0.5 | 1 | 19.514 | 18.798 | 18.566 | 18.581 | 18.832 | 18.857 | 18.727 | 18.279 |
| | | 2 | 20.824 | 20.395 | 20.251 | 20.254 | 20.350 | 20.251 | 20.036 | 19.506 |
| | | 3 | 24.025 | 23.384 | 23.187 | 23.231 | 23.451 | 23.383 | 23.147 | 22.504 |
| | 1 | 1 | 34.147 | 33.085 | 32.772 | 32.868 | 33.329 | 33.306 | 32.972 | 31.985 |
| | | 2 | 44.671 | 43.461 | 43.103 | 43.221 | 43.719 | 43.614 | 43.142 | 41.844 |
| | | 3 | 49.402 | 47.658 | 47.199 | 47.501 | 48.476 | 48.513 | 47.970 | 46.274 |
| | 1.5 | 1 | 48.641 | 47.326 | 46.904 | 46.939 | 47.371 | 47.268 | 46.811 | 45.562 |
| | | 2 | 70.269 | 67.712 | 67.073 | 67.597 | 69.159 | 69.243 | 68.417 | 65.819 |
| | | 3 | 74.884 | 72.874 | 72.252 | 72.370 | 73.102 | 72.927 | 72.181 | 70.144 |
| | 2 | 1 | 64.090 | 62.552 | 62.008 | 61.925 | 62.227 | 62.018 | 61.461 | 60.033 |
| | | 2 | 87.781 | 84.554 | 83.765 | 84.470 | 86.515 | 86.634 | 85.570 | 82.223 |
| | | 3 | 96.001 | 93.038 | 92.194 | 92.541 | 93.944 | 93.872 | 92.866 | 89.923 |
| $\pi/2$ | 0.5 | 1 | 17.098 | 16.440 | 16.226 | 16.234 | 16.461 | 16.497 | 16.396 | 16.015 |
| | | 2 | 18.125 | 17.818 | 17.698 | 17.661 | 17.658 | 17.547 | 17.369 | 16.979 |
| | | 3 | 18.557 | 18.038 | 17.826 | 17.787 | 17.870 | 17.821 | 17.698 | 17.383 |
| | 1 | 1 | 29.451 | 28.607 | 28.338 | 28.365 | 28.653 | 28.607 | 28.340 | 27.586 |
| | | 2 | 30.534 | 29.536 | 29.248 | 29.356 | 29.823 | 29.821 | 29.518 | 28.601 |
| | | 3 | 34.757 | 33.950 | 33.683 | 33.700 | 33.913 | 33.778 | 33.433 | 32.557 |
| | 1.5 | 1 | 40.088 | 38.894 | 38.536 | 38.630 | 39.128 | 39.084 | 38.689 | 37.550 |
| | | 2 | 41.046 | 39.967 | 39.608 | 39.610 | 39.893 | 39.781 | 39.419 | 38.447 |
| | | 3 | 49.474 | 47.942 | 47.504 | 47.675 | 48.415 | 48.391 | 47.870 | 46.341 |
| | 2 | 1 | 49.438 | 48.087 | 47.656 | 47.698 | 48.154 | 48.053 | 47.588 | 46.308 |
| | | 2 | 51.951 | 50.469 | 50.014 | 50.114 | 50.641 | 50.533 | 50.043 | 48.662 |
| | | 3 | 63.899 | 62.314 | 61.771 | 61.721 | 62.138 | 61.971 | 61.385 | 59.853 |

Table 8: Fundamental frequency parameters for FGOS with two axial bulkheads and various boundary conditions ($R = 1$ m, $L_1/R = 2$, $d/R = 0.5$, $2\theta_1 = \theta_2 = 2\theta_3 = \pi/4$).

| $h/R$ | $\alpha$ | $p$ | Boundary conditions | | | | | | | |
|---|---|---|---|---|---|---|---|---|---|---|
| | | | CCCC | CSCS | CFCF | FCFC | CECE | ECEC | ESES | EEEE |
| $FGM_I$ ($a = 1/b = 0.5/c = 2$) | | | | | | | | | | |
| 0.05 | $\pi/6$ | 0.5 | 32.474 | 28.651 | 14.631 | 17.548 | 29.315 | 31.868 | 27.905 | 28.628 |
| | | 1 | 32.327 | 28.523 | 14.580 | 17.462 | 29.187 | 31.724 | 27.783 | 28.507 |
| | | 10 | 31.596 | 27.924 | 14.511 | 17.081 | 28.576 | 31.028 | 27.234 | 27.947 |
| | $\pi/3$ | 0.5 | 19.869 | 18.863 | 11.618 | 8.743 | 19.083 | 19.535 | 18.693 | 18.934 |
| | | 1 | 19.782 | 18.782 | 11.578 | 8.705 | 19.002 | 19.451 | 18.614 | 18.855 |
| | | 10 | 19.424 | 18.473 | 11.535 | 8.591 | 18.689 | 19.114 | 18.319 | 18.552 |
| 0.1 | $\pi/6$ | 0.5 | 22.967 | 21.159 | 13.575 | 12.674 | 21.366 | 22.721 | 20.881 | 21.095 |
| | | 1 | 22.873 | 21.076 | 13.524 | 12.613 | 21.283 | 22.629 | 20.799 | 21.014 |
| | | 10 | 22.493 | 20.779 | 13.446 | 12.357 | 20.982 | 22.262 | 20.516 | 20.728 |
| | $\pi/3$ | 0.5 | 15.583 | 15.207 | 10.966 | 7.301 | 15.300 | 15.457 | 15.163 | 15.258 |
| | | 1 | 15.522 | 15.149 | 10.925 | 7.270 | 15.241 | 15.397 | 15.105 | 15.200 |
| | | 10 | 15.353 | 15.001 | 10.873 | 7.192 | 15.092 | 15.235 | 14.960 | 15.053 |
| $FGM_{II}$ ($a = 1/b = 0.5/c = 2$) | | | | | | | | | | |
| 0.05 | $\pi/6$ | 0.5 | 32.469 | 28.648 | 14.633 | 17.546 | 29.310 | 31.863 | 27.903 | 28.623 |
| | | 1 | 32.317 | 28.518 | 14.584 | 17.460 | 29.178 | 31.715 | 27.779 | 28.498 |
| | | 10 | 31.578 | 27.912 | 14.519 | 17.076 | 28.558 | 31.010 | 27.225 | 27.931 |
| | $\pi/3$ | 0.5 | 19.871 | 18.866 | 11.622 | 8.745 | 19.085 | 19.537 | 18.697 | 18.936 |
| | | 1 | 19.786 | 18.788 | 11.585 | 8.708 | 19.006 | 19.455 | 18.620 | 18.859 |
| | | 10 | 19.430 | 18.482 | 11.547 | 8.597 | 18.693 | 19.119 | 18.328 | 18.557 |
| 0.1 | $\pi/6$ | 0.5 | 22.961 | 21.155 | 13.582 | 12.673 | 21.359 | 22.715 | 20.877 | 21.088 |
| | | 1 | 22.862 | 21.067 | 13.537 | 12.610 | 21.270 | 22.618 | 20.792 | 21.002 |
| | | 10 | 22.471 | 20.761 | 13.468 | 12.353 | 20.956 | 22.240 | 20.500 | 20.704 |
| | $\pi/3$ | 0.5 | 15.587 | 15.213 | 10.975 | 7.305 | 15.304 | 15.461 | 15.168 | 15.262 |
| | | 1 | 15.529 | 15.158 | 10.941 | 7.278 | 15.248 | 15.404 | 15.114 | 15.207 |
| | | 10 | 15.363 | 15.015 | 10.900 | 7.205 | 15.101 | 15.245 | 14.975 | 15.063 |

Table 9: Fundamental frequency parameters for FGOS with two circumferential bulkheads and various boundary conditions ($R = 1$ m, $L_1 = L_2 = L_3 = 1$ m, $d/R = 0.5$, $\theta_1 = \pi/2$).

| $h/R$ | $\alpha$ | $p$ | Boundary conditions | | | | | | | |
|---|---|---|---|---|---|---|---|---|---|---|
| | | | CCCC | SCSC | CFCF | FCFC | CECE | ECEC | SESE | EEEE |
| $FGM_I$ ($a = 1/b = 0.5/c = 2$) | | | | | | | | | | |
| 0.05 | $\pi/6$ | 0.5 | 79.218 | 68.455 | 53.402 | 30.933 | 76.759 | 78.935 | 66.379 | 76.704 |
| | | 1 | 78.899 | 68.167 | 53.194 | 30.818 | 76.437 | 78.619 | 66.095 | 76.382 |
| | | 10 | 77.512 | 66.777 | 52.723 | 30.371 | 74.998 | 77.255 | 64.658 | 74.942 |
| | $\pi/3$ | 0.5 | 56.969 | 44.835 | 47.938 | 18.335 | 56.604 | 56.835 | 42.124 | 56.321 |
| | | 1 | 56.738 | 44.665 | 47.756 | 18.264 | 56.372 | 56.608 | 41.990 | 56.096 |
| | | 10 | 55.959 | 44.031 | 47.461 | 17.880 | 55.582 | 55.850 | 41.434 | 55.340 |
| 0.1 | $\pi/6$ | 0.5 | 58.299 | 47.463 | 45.867 | 21.764 | 56.685 | 57.846 | 43.033 | 54.433 |
| | | 1 | 58.058 | 47.282 | 45.668 | 21.680 | 56.430 | 57.620 | 42.852 | 54.180 |
| | | 10 | 57.041 | 46.391 | 45.166 | 21.277 | 55.358 | 56.607 | 41.769 | 52.880 |
| | $\pi/3$ | 0.5 | 46.856 | 36.926 | 43.045 | 13.259 | 46.534 | 46.761 | 27.154 | 45.758 |
| | | 1 | 46.662 | 36.815 | 42.860 | 13.202 | 46.340 | 46.568 | 27.075 | 45.569 |
| | | 10 | 46.172 | 36.509 | 42.486 | 12.912 | 45.856 | 46.070 | 26.611 | 44.851 |
| $FGM_{II}$ ($a = 1/b = 0.5/c = 2$) | | | | | | | | | | |
| 0.05 | $\pi/6$ | 0.5 | 79.168 | 68.407 | 53.434 | 30.907 | 76.728 | 78.884 | 66.335 | 76.676 |
| | | 1 | 78.807 | 68.083 | 53.253 | 30.770 | 76.381 | 78.526 | 66.015 | 76.330 |
| | | 10 | 77.366 | 66.639 | 52.821 | 30.294 | 74.909 | 77.108 | 64.526 | 74.860 |
| | $\pi/3$ | 0.5 | 56.976 | 44.806 | 47.980 | 18.325 | 56.616 | 56.836 | 42.090 | 56.326 |
| | | 1 | 56.751 | 44.611 | 47.831 | 18.245 | 56.394 | 56.611 | 41.929 | 56.106 |
| | | 10 | 55.983 | 43.942 | 47.583 | 17.854 | 55.621 | 55.861 | 41.332 | 55.362 |
| 0.1 | $\pi/6$ | 0.5 | 58.277 | 47.393 | 45.932 | 21.736 | 56.707 | 57.793 | 42.984 | 54.453 |
| | | 1 | 58.019 | 47.154 | 45.786 | 21.629 | 56.469 | 57.524 | 42.764 | 54.217 |
| | | 10 | 56.983 | 46.177 | 45.360 | 21.194 | 55.422 | 56.449 | 41.623 | 52.941 |
| | $\pi/3$ | 0.5 | 46.899 | 36.865 | 43.116 | 13.249 | 46.582 | 46.801 | 27.122 | 45.780 |
| | | 1 | 46.740 | 36.703 | 42.991 | 13.185 | 46.427 | 46.641 | 27.015 | 45.608 |
| | | 10 | 46.299 | 36.324 | 42.698 | 12.885 | 45.996 | 46.189 | 26.514 | 44.885 |

b = −0.5/$c = p = 2$) open shell with two bulkheads. All boundaries of the shell are clamped and the geometrical dimensions are as follows:

FGOS with two axial bulkheads: $R = 1$ m, $L/R = 2$, $h/R = 0.05$, $\theta_1 = \theta_2 = \theta_3 = \pi/6$.

FGOS with two circumferential bulkheads: $R = 1$ m, $h/R = 0.05$, $2L_1 = L_2 = 2L_3 = 1$m, $\theta_1 = \pi/2$.

From Figure 10, it can be seen that the frequency parameters decrease as the height of the bulkhead increases. It means that the overall stiffness of the structure decreases as the height of the plate increases.

Next, research on the vibration characteristics of bulkhead-stiffened FGOS with different geometries and boundary conditions is conducted. Tables 6 and 7 show the frequency parameters of FGOS with one axial and circumferential bulkheads according to the power law index. In Tables 6 and 7, the frequency parameters of FGOS decrease as the power law index increase. In addition, when the circumferential size $\theta_1$ of the shell increase, the frequency parameters decrease because the stiffness of the structure decreases as the geometric dimensions increase. Tables 8 and 9 show the frequency parameters of FGOS with two bulkheads and different boundary conditions. The results in Tables 6–9 can be used as benchmark data for researchers in this field.

## 4. Conclusions

In this paper, the free vibration analysis of bulkhead-stiffened FGOS with various geometry and boundary conditions is performed by a meshless Legendre-RPIM shape function that uses a combined basis of Legendre polynomials and MQ radial functions. A bulkhead-stiffened FGOS is decomposed into several shells and bulkheads, and the governing equations and boundary conditions of each segment are derived from Hamilton's principle and FSDT. Continuous conditions of displacement are applied at the interfaces between the segments. In order to solve these equations, the meshless strong form method is adopted. In the equations discretized by the meshless strong form method, the displacement components are approximated by the Legendre-RPIM shape function, and the boundary and continuous conditions are applied using artificial spring technology. The accuracy and reliability of the proposed method for free vibration analysis of bulkhead-stiffened FGOS are confirmed through the convergence study and comparison with the results of pieces of literature and ABAQUS. The effects of the geometry of bulkhead, parameters of material composition, and boundary conditions on the frequency parameters of bulkhead-stiffened FGOS are investigated through some numerical examples, and these results can be used as benchmark data for research in this field.

## Appendix

## A. Detailed Expressions of the Constants $L_{ij}$

$L_{11}$

$$
\begin{aligned}
L_{12} &= Q(A_{12} + A_{66})\frac{\partial^2}{\partial x \partial \beta} + (PQA_{12} - PQA_{11} - PQA_{66})\frac{\partial}{\partial \beta},\\
L_{13} &= SA_{12}\frac{\partial}{\partial x} + PS(A_{12} - A_{11}),\\
L_{15} &= L_{42} = Q(B_{12} + B_{66})\frac{\partial^2}{\partial x \partial \beta} + (PQB_{12} - PQB_{11} - PQB_{66})\frac{\partial}{\partial \beta},\\
L_{21} &= Q(A_{12} + A_{66})\frac{\partial^2}{\partial x \partial \beta} + (PQA_{11} + 2PQA_{66})\frac{\partial}{\partial \beta},\\
L_{22} &= A_{66}\frac{\partial^2}{\partial x^2} + Q^2A_{11}\frac{\partial^2}{\partial \beta^2} + PA_{66}\frac{\partial}{\partial x} - 2P^2A_{66} - S^2A_{44},\\
L_{23} &= QS(A_{11} + A_{44})\frac{\partial}{\partial \beta},\\
L_{24} &= L_{51} = Q(B_{12} + B_{66})\frac{\partial^2}{\partial x \partial \beta} + (PQB_{11} + 2PQB_{66})\frac{\partial}{\partial \beta},\\
L_{25} &= L_{52} = B_{66}\frac{\partial^2}{\partial x^2} + Q^2B_{11}\frac{\partial^2}{\partial \beta^2} + PB_{66}\frac{\partial}{\partial x} - 2P^2B_{66} + SA_{44},\\
L_{31} &= -SA_{12}\frac{\partial}{\partial x} - PSA_{11},\\
L_{32} &= -SQ(A_{11} + A_{44})\frac{\partial}{\partial \beta},\\
L_{33} &= A_{55}\frac{\partial^2}{\partial x^2} + Q^2A_{44}\frac{\partial^2}{\partial \beta^2} + PA_{55}\frac{\partial}{\partial x} - S^2A_{11},\\
L_{34} &= (A_{55} - SB_{12})\frac{\partial}{\partial x} + P(A_{55} - SB_{11}),\\
L_{35} &= Q(A_{44} - SB_{11})\frac{\partial}{\partial \beta},\\
L_{43} &= (-A_{55} + SB_{12})\frac{\partial}{\partial x} + PS(B_{12} - B_{11}),\\
L_{44} &= D_{11}\frac{\partial^2}{\partial x^2} + Q^2D_{66}\frac{\partial^2}{\partial \beta^2} + PD_{11}\frac{\partial}{\partial x} + P^2D_{12} - P^2D_{11} - A_{55},\\
L_{45} &= Q(D_{12} + D_{66})\frac{\partial^2}{\partial x \partial \beta} + (PQD_{12} - PQD_{11} - PQD_{66})\frac{\partial}{\partial \beta},\\
L_{53} &= Q(-A_{44} + SB_{11})\frac{\partial}{\partial \beta},\\
L_{54} &= Q(D_{12} + D_{66})\frac{\partial^2}{\partial x \partial \beta} + (PQD_{11} + 2PQD_{66})\frac{\partial}{\partial \beta},\\
L_{55} &= D_{66}\frac{\partial^2}{\partial x^2} + Q^2D_{11}\frac{\partial^2}{\partial \beta^2} + PD_{66}\frac{\partial}{\partial x} - 2P^2D_{66} - A_{44}.
\end{aligned}
\tag{A.1}
$$

## B. Detailed Expressions of the Constants $C_{xij}$

$$
\begin{aligned}
&C_{x11}\\
&C_{x12} = QA_{12}\frac{\partial}{\partial\beta}, \quad C_{x33} = A_{55}\frac{\partial}{\partial x} \pm k_w^x,\\
&C_{x13} = SA_{12}, \quad C_{x34} = A_{55},\\
&C_{x14} = C_{x41} = B_{11}\frac{\partial}{\partial x} + PB_{12}, \quad C_{x43} = SB_{12},\\
&C_{x15} = C_{x42} = QB_{12}\frac{\partial}{\partial\beta}, \quad C_{x44} = D_{11}\frac{\partial}{\partial x} + PD_{12} \pm k_x^x,\\
&C_{x21} = QA_{66}\frac{\partial}{\partial\beta}, \quad C_{x45} = QD_{12}\frac{\partial}{\partial\beta},\\
&C_{x22} = A_{66}\frac{\partial}{\partial x} - PA_{66} \pm k_v^x, \quad C_{x54} = QD_{66}\frac{\partial}{\partial\beta},\\
&C_{x23} = C_{x31} = C_{x32} = C_{x35} = C_{x53} = 0, \quad C_{x55} = D_{66}\frac{\partial}{\partial x} - PD_{66} \pm k_\beta^x,\\
&C_{x24} = C_{x51} = QB_{66}\frac{\partial}{\partial\beta},\\
&C_{\beta11} = QA_{66}\frac{\partial}{\partial\beta} \pm k_u^\beta, \quad C_{\beta25} = C_{\beta52} = QB_{11}\frac{\partial}{\partial\beta},\\
&C_{\beta12} = A_{66}\frac{\partial}{\partial x} - PA_{66}, \quad C_{\beta32} = -SA_{44},\\
&C_{\beta13} = C_{x31} = C_{\beta34} = C_{\beta43} = 0, \quad C_{\beta33} = QA_{44}\frac{\partial}{\partial\beta} \pm k_w^\beta,\\
&C_{\beta14} = C_{\beta41} = QB_{66}\frac{\partial}{\partial\beta}, \quad C_{\beta35} = A_{44},\\
&C_{\beta15} = C_{\beta42} = B_{66}\frac{\partial}{\partial x} - PB_{66}, \quad C_{\beta44} = QD_{66}\frac{\partial}{\partial\beta} \pm k_x^\beta,\\
&C_{\beta21} = A_{12}\frac{\partial}{\partial x} + PA_{11}, \quad C_{\beta45} = D_{66}\frac{\partial}{\partial x} - PD_{66},\\
&C_{\beta22} = QA_{11}\frac{\partial}{\partial\beta} \pm k_v^\beta, \quad C_{\beta53} = SB_{11},\\
&C_{\beta23} = SA_{11}, \quad C_{\beta54} = D_{12}\frac{\partial}{\partial x} + PD_{11},\\
&C_{\beta24} = C_{\beta51} = B_{12}\frac{\partial}{\partial x} + PB_{11}, \quad C_{\beta55} = QD_{11}\frac{\partial}{\partial\beta} \pm k_\beta^\beta,
\end{aligned}
\tag{B.1}
$$

## Data Availability

The data that support the findings of this study are included within the article.

## Conflicts of Interest

The authors declare that there are no conflicts of interest regarding the publication of this paper.

## Acknowledgments

The authors would like to take the opportunity to express their hearted gratitude to all those who make a contribution to the completion of this article.

## References

[1] S. Zhu, G. Jin, and T. Ye, "Free vibration analysis of moderately thick functionally graded open shells with general boundary conditions," *Composite Structures*, vol. 117, pp. 169–186, 2014.

[2] A. R. Saidi, A. H. Baferani, and E. Jomehzadeh, "Benchmark solution for free vibration of functionally graded moderately thick annular sector plates," *Acta Mechanica*, vol. 219, no. 3-4, pp. 309–335, 2011.

[3] J. Rouzegar and F. Abad, "Free vibration analysis of FG plate with piezoelectric layers using four-variable refined plate theory," *Thin-Walled Structures*, vol. 89, pp. 76–83, 2015.

[4] S. Chakraverty and K. K. Pradhan, "Free vibration of exponential functionally graded rectangular plates in thermal environment with general boundary conditions," *Aerospace Science and Technology*, vol. 36, pp. 132–156, 2014.

[5] S. Natarajan, P. M. Baiz, M. Ganapathi, P. Kerfriden, and S. Bordas, "Linear free flexural vibration of cracked functionally graded plates in thermal environment," *Computers & Structures*, vol. 89, no. 15-16, pp. 1535–1546, 2011.

[6] H. Bagheri, Y. Kiani, and M. R. Eslami, "Free vibration of joined conical-conical shells," *Thin-Walled Structures*, vol. 120, pp. 446–457, 2017.

[7] H. Bagheri, Y. Kiani, and M. R. Eslami, "Free vibration of joined conical-cylindrical-conical shells," *Acta Mechanica*, vol. 229, no. 7, pp. 2751–2764, 2018.

[8] H. Bagheri, Y. Kiani, N. Bagheri, and M. R. Eslami, "Free vibrations of functionally graded material cylindrical shell closed with two spherical caps," *Ships and Offshore Structures*, vol. 17, no. 4, pp. 939–951, 2022.

[9] H. Bagheri, Y. Kiani, and M. R. Eslami, "Free vibration of FGM conical–spherical shells," *Thin-Walled Structures*, vol. 160, Article ID 107387, 2021.

[10] Q. Wang, F. Xie, B. Qin, R. Zhong, and H. Yu, "Dynamics and power flow control of irregular elastic coupled plate systems: precise modeling and experimental validation," *International Journal of Mechanical Sciences*, vol. 185, Article ID 105760, 2020.

[11] Z. Su, G. Jin, and T. Ye, "Three-dimensional vibration analysis of thick functionally graded conical, cylindrical shell and annular plate structures with arbitrary elastic restraints," *Composite Structures*, vol. 118, pp. 432–447, 2014.

[12] G. Jin, Z. Su, T. Ye, and S. Gao, "Three-dimensional free vibration analysis of functionally graded annular sector plates with general boundary conditions," *Composites Part B: Engineering*, vol. 83, pp. 352–366, 2015.

[13] S. Khare and N. D. Mittal, "Free vibration of thick laminated circular and annular plates using three-dimensional finite element analysis," *Alexandria Engineering Journal*, vol. 57, no. 3, pp. 1217–1228, 2018.

[14] T. Xiang, S. Natarajan, H. Man, C. Song, and W. Gao, "Free vibration and mechanical buckling of plates with in-plane material inhomogeneity - a three dimensional consistent approach," *Composite Structures*, vol. 118, pp. 634–642, 2014.

[15] T. Liu, G. Hu, A. Wang, and Q. Wang, "A unified formulation for free in-plane vibrations of arbitrarily-shaped straight-sided quadrilateral and triangular thin plates," *Applied Acoustics*, vol. 155, pp. 407–422, 2019.

[16] F. Ebrahimi and A. Rastgo, "An analytical study on the free vibration of smart circular thin FGM plate based on classical plate theory," *Thin-Walled Structures*, vol. 46, no. 12, pp. 1402–1408, 2008.

[17] D. Shao, Q. Wang, C. Shuai, and J. Gu, "Investigation on dynamic performances of a set of composite laminated plate system under the influences of boundary and coupling conditions," *Mechanical Systems and Signal Processing*, vol. 132, pp. 721–747, 2019.

[18] H. Bagheri, Y. Kiani, and M. R. Eslami, "Free vibration of conical shells with intermediate ring support," *Aerospace Science and Technology*, vol. 69, pp. 321–332, 2017.

[19] S. Natarajan, G. Manickam, and S. Bordas, "Supersonic flutter analysis of functionally graded material plates with cracks," *Frontiers of Aerospace Engineering*, vol. 2, no. 2, pp. 91–97, 2013.

[20] J. L. Mantari, A. S. Oktem, and C. Guedes Soares, "A new higher order shear deformation theory for sandwich and composite laminated plates," *Composites Part B: Engineering*, vol. 43, no. 3, pp. 1489–1499, 2012.

[21] M. Mohammadi, E. Mohseni, and M. Moeinfar, "Bending, buckling and free vibration analysis of incompressible functionally graded plates using higher order shear and normal deformable plate theory," *Applied Mathematical Modelling*, vol. 69, pp. 47–62, 2019.

[22] S. Merdaci and H. Belghoul, "High-order shear theory for static analysis of functionally graded plates with porosities," *Comptes Rendus Mecanique*, vol. 347, no. 3, pp. 207–217, 2019.

[23] J. L. Mantari, A. S. Oktem, and C. Guedes Soares, "Static and dynamic analysis of laminated composite and sandwich plates and shells by using a new higher-order shear deformation theory," *Composite Structures*, vol. 94, no. 1, pp. 37–49, 2011.

[24] J. H. Kang and A. W. Leissa, "Three-dimensional vibration analysis of thick hyperboloidal shells of revolution," *Journal of Sound and Vibration*, vol. 282, no. 1-2, pp. 277–296, 2005.

[25] Y. Qu, X. Long, G. Yuan, and G. Meng, "A unified formulation for vibration analysis of functionally graded shells of revolution with arbitrary boundary conditions," *Composites Part B: Engineering*, vol. 50, pp. 381–402, 2013.

[26] X. Xie, H. Zheng, and G. Jin, "Free vibration of four-parameter functionally graded spherical and parabolic shells of revolution with arbitrary boundary conditions," *Composites Part B: Engineering*, vol. 77, pp. 59–73, 2015.

[27] F. Pang, H. Li, X. Wang, X. Miao, and S. Li, "A semi analytical method for the free vibration of doubly-curved shells of revolution," *Computers & Mathematics with Applications*, vol. 75, no. 9, pp. 3249–3268, 2018.

[28] B. Bediz, "A spectral-Tchebychev solution technique for determining vibrational behavior of thick plates having arbitrary geometry," *Journal of Sound and Vibration*, vol. 432, pp. 272–289, 2018.

[29] T. Ye, G. Jin, Z. Su, and X. Jia, "A unified Chebyshev–Ritz formulation for vibration analysis of composite laminated deep open shells with arbitrary boundary conditions," *Archive of Applied Mechanics*, vol. 84, no. 4, pp. 441–471, 2014.

[30] B. Qin, R. Zhong, T. Wang, Q. Wang, Y. Xu, and Z. Hu, "A unified Fourier series solution for vibration analysis of FG-CNTRC cylindrical, conical shells and annular plates with arbitrary boundary conditions," *Composite Structures*, vol. 232, Article ID 111549, 2020.

[31] N. Nguyen-Thanh, T. Rabczuk, H. Nguyen-Xuan, and S. P. A. Bordas, "A smoothed finite element method for shell analysis," *Computer Methods in Applied Mechanics and Engineering*, vol. 198, no. 2, pp. 165–177, 2008.

[32] M. Barik and M. Mukhopadhyay, "Finite element free flexural vibration analysis of arbitrary plates," *Finite Elements in Analysis and Design*, vol. 29, no. 2, pp. 137–151, 1998.

[33] S. Natarajan, A. J. M. Ferreira, S. Bordas, E. Carrera, M. Cinefra, and A. M. Zenkour, "Analysis of functionally graded material plates using triangular elements with cell-based smoothed discrete shear gap method," *Mathematical Problems in Engineering*, pp. 1–13, Article ID 247932, 2014.

[34] N. Fantuzzi, F. Tornabene, and E. Viola, "Four-parameter functionally graded cracked plates of arbitrary shape: a GDQFEM solution for free vibrations," *Mechanics of Advanced Materials and Structures*, vol. 23, no. 1, pp. 89–107, 2016.

[35] T. Ye, G. Jin, Y. Chen, and S. Shi, "A unified formulation for vibration analysis of open shells with arbitrary boundary conditions," *International Journal of Mechanical Sciences*, vol. 81, pp. 42–59, 2014.

[36] Y. Xue, G. Jin, X. Ma et al., "Free vibration analysis of porous plates with porosity distributions in the thickness and in-plane directions using isogeometric approach," *International Journal of Mechanical Sciences*, vol. 152, pp. 346–362, 2019.

[37] S. Kumar, V. Ranjan, and P. Jana, "Free vibration analysis of thin functionally graded rectangular plates using the dynamic stiffness method," *Composite Structures*, vol. 197, pp. 39–53, 2018.

[38] R. Talebitooti and V. S. Anbardan, "Haar wavelet discretization approach for frequency analysis of the functionally graded generally doubly-curved shells of revolution," *Applied Mathematical Modelling*, vol. 67, pp. 645–675, 2019.

[39] G. R. Liu and Y. T. Gu, *An Introduction to Meshfree Methods and Their Programming*, Springer, Dordrecht, 2005.

[40] A. Zarei and A. Khosravifard, "Meshfree investigation of the vibrational behavior of pre-stressed laminated composite plates based on a variationally consistent plate model," *Engineering Analysis with Boundary Elements*, vol. 111, pp. 118–133, 2020.

[41] N. Fallah and M. Delzendeh, "Free vibration analysis of laminated composite plates using meshless finite volume method," *Engineering Analysis with Boundary Elements*, vol. 88, pp. 132–144, 2018.

[42] T. V. Vu, A. Khosravifard, M. R. Hematiyan, and T. Q. Bui, "A new refined simple TSDT-based effective meshfree method for analysis of through-thickness FG plates," *Applied Mathematical Modelling*, vol. 57, pp. 514–534, 2018.

[43] L. W. Zhang, Z. X. Lei, and K. M. Liew, "Free vibration analysis of functionally graded carbon nanotube-reinforced composite triangular plates using the FSDT and element-free IMLS-Ritz method," *Composite Structures*, vol. 120, pp. 189–199, 2015.

[44] A. Stanley and N. Ganesan, "Frequency response of shell-plate combinations," *Computers & Structures*, vol. 59, no. 6, pp. 1083–1094, 1996.

[45] Y. Qu, H. Hua, and G. Meng, "Vibro-acoustic analysis of coupled spherical–cylindrical–spherical shells stiffened by ring and stringer reinforcements," *Journal of Sound and Vibration*, vol. 355, pp. 345–359, 2015.

[46] M. Chen, J. Wei, K. Xie, N. Deng, and G. Hou, "Wave based method for free vibration analysis of ring stiffened cylindrical shell with intermediate large frame ribs," *Shock and Vibration*, vol. 20, no. 3, pp. 459–479, 2013.

[47] S. Kwak, K. Kim, J. Kim, Y. Kim, Y. Kim, and K. Pang, "A meshfree approach for free vibration analysis of laminated sectorial and rectangular plates with varying fiber angle," *Thin-Walled Structures*, vol. 174, Article ID 109070, 2022.

[48] Y. F. Xing, Y. Wu, Bo Liu, A. J. M. Ferreira, and A. M. A. Neves, "Static and dynamic analyses of laminated plates using a layerwise theory and a radial basis function finite element method," *Composite Structures*, vol. 170, pp. 158–168, 2017.

[49] Y. Kiani, M. Shakeri, and M. R. Eslami, "Thermoelastic free vibration and dynamic behaviour of an FGM doubly curved panel via the analytical hybrid Laplace–Fourier transformation," *Acta Mechanica*, vol. 223, no. 6, pp. 1199–1218, 2012.